AD-A131 035 ATMOSPHERIC IR TRANSMISSION DATA FOR A TEMPERATE MARITIME ENVIRONMENT(U) ELECTRONICS RESEARCH LAB ADELAIDE (AUSTRALIA) D R CUTTEN FEB 83 ERL-0265-TR F/G 4/1 1/1

UNCLASSIFIED NL

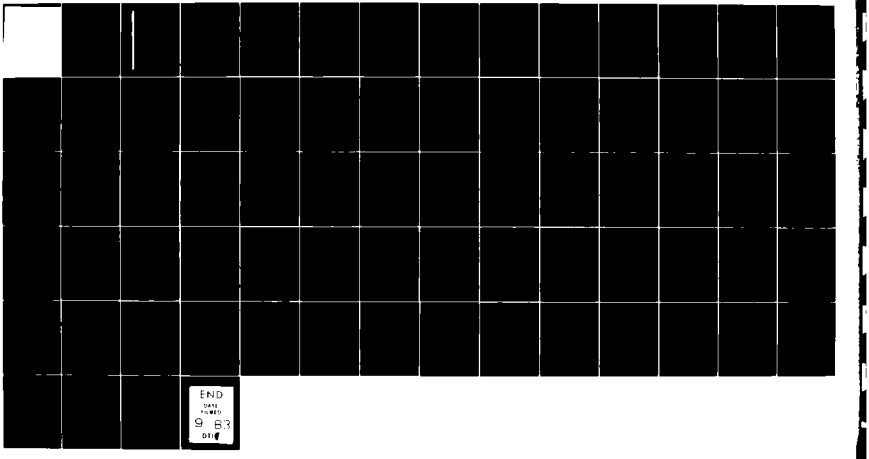

END
DATE FILMED
9 83
DTIC

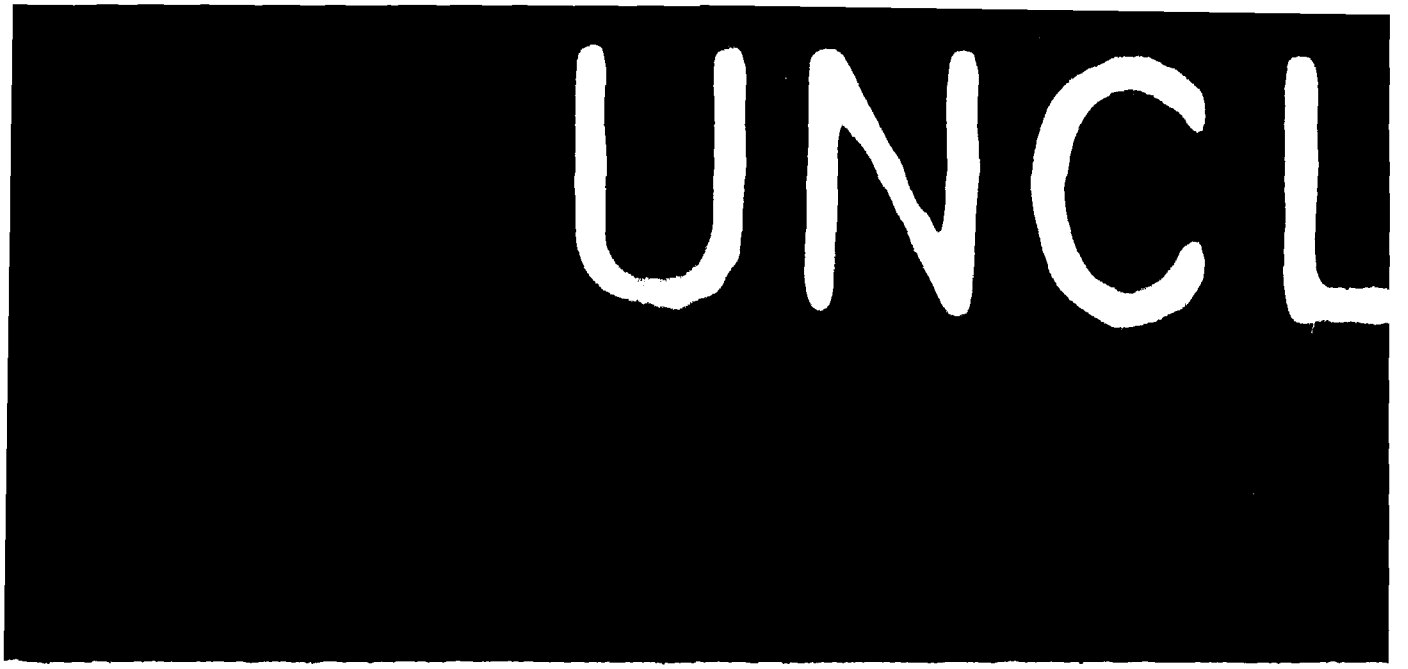
UNCL

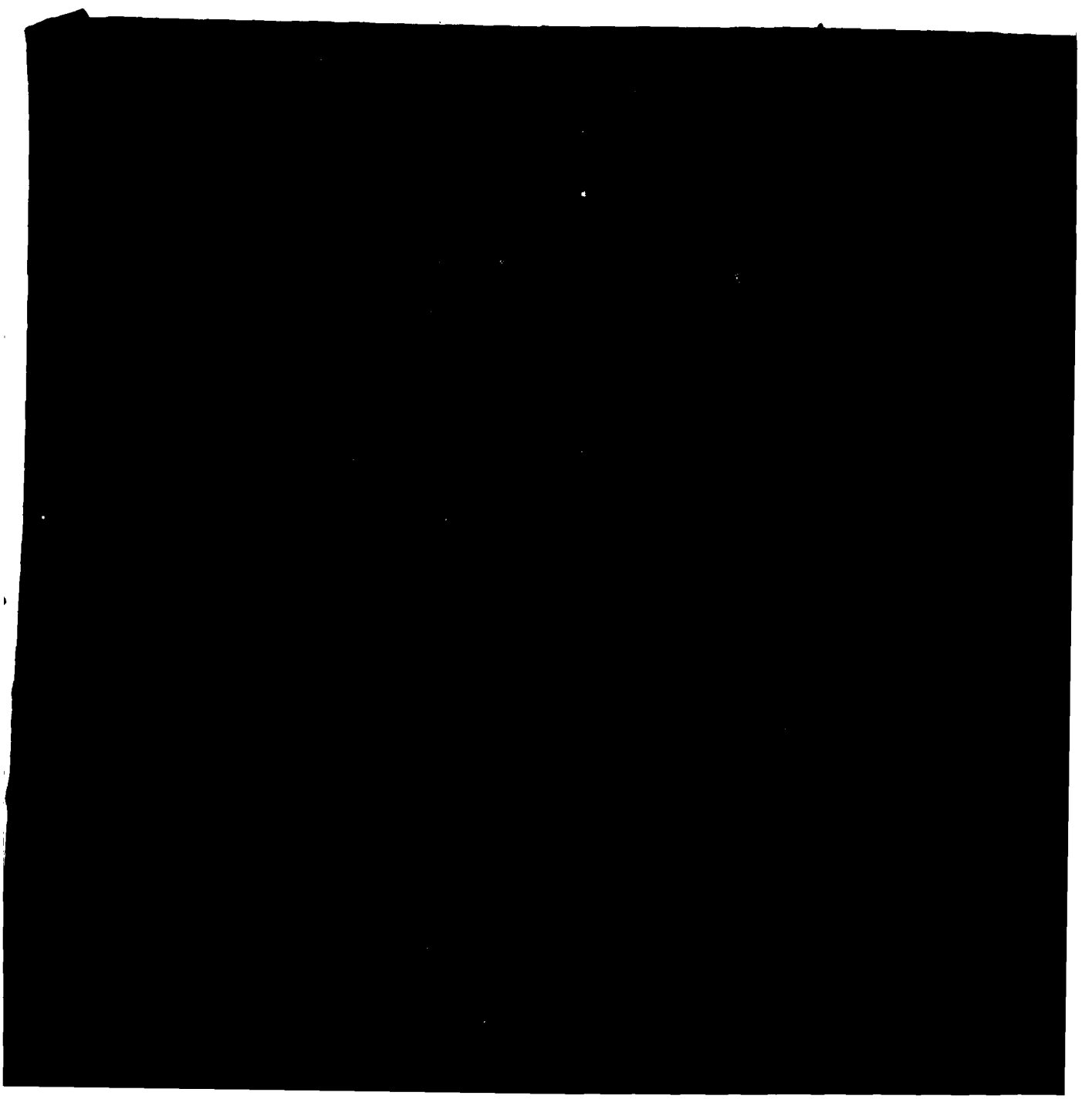

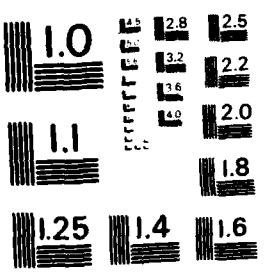

ERL-0265-TR

AR-003-098

AUSTRALIA

DEPARTMENT OF DEFENCE

DEFENCE SCIENCE AND TECHNOLOGY ORGANISATION

ELECTRONICS RESEARCH LABORATORY

DEFENCE RESEARCH CENTRE SALISBURY
SOUTH AUSTRALIA

AD A131038

TECHNICAL REPORT

ERL-0265-TR

ATMOSPHERIC IR TRANSMISSION DATA FOR A TEMPERATE MARITIME ENVIRONMENT

D.R. CUTTEN

DTIC FILE COPY

DTIC ELECTE AUG 4 1983 D

Approved for Public Release

COPY No.

FEBRUARY 1983

UNCLASSIFIED

AR-

DEPARTMENT OF DEFENCE

DEFENCE SCIENCE AND TECHNOLOGY ORGANISATION

ELECTRONICS RESEARCH LABORATORY

TECHNICAL REPORT

ERL-0265-TR

ATMOSPHERIC IR TRANSMISSION DATA FOR A TEMPERATE MARITIME ENVIRONMENT

D.R. Cutten

S U M M A R Y

Measurements are reported on infrared transmission through the atmosphere at a coastal marine site in a temperate environment. Ten broadband spectral regions were used and variations of transmittance with absolute humidity and visibility over paths of 5 and 9 km investigated. All data have been compared with the predictions of the AFGL computer code LOWTRAN 5. The discrepancy reported previously between the measured and calculated data in the 4.4 to 5.4 μm region still exists, although new data on the water continuum absorption coefficients for this region have reduced this. Reasonable agreement has been shown to exist in the 8 to 12 μm region for absolute humidities up to 12 gm/m^3. The results of the comparisons for the 1 to 2.5 μm region showed a greater discrepancy. Some of this discrepancy could be arising from point measurements of aerosol extinction using equipment which is underestimating the aerosol attenuation coefficient. Data on scintillation fluctuations recorded during the transmittance measurements are also presented.

POSTAL ADDRESS: Director, Electronics Research Laboratory,
Box 2151, GPO, Adelaide, South Australia, 5001.

TABLE OF CONTENTS

LIST OF TABLES

Page

LIST OF FIGURES

LIST OF APPENDICES

1. INTRODUCTION

Data on broadband infrared (IR) atmospheric transmittance have been collected over long paths near the air-sea interface in a temperate environment during the period November 1977 to December 1979. This work was carried out under task NAVY 77/141 which involved a study of the parameters affecting IR atmospheric transmittance near the air-sea interface. Such data in particular, are required to verify the predictions of atmospheric transmittance models e.g. the AFGL computer code LOWTRAN 5, under similar meteorological conditions(ref.1). The operating capabilities of IR surveillance, missile and countermeasure equipment in the environments encountered around Australia are most important to Australia's defence and the evaluation of such systems generally depend on the use of atmospheric transmittance models to predict the optical properties of the intervening atmosphere. Hence the need exists to validate the predictions of models over long ranges in Australian environments.

A preliminary assessment of transmittance data measured at the coastal marine site over the period November 1977 to April 1978 has already been reported(ref.2). It is the purpose of this paper to report on the analysis of transmittance data measured during the period October 1978 to December 1979. Data are included for ten broadband spectral regions from 1 to 12 μm and the effects of absolute humidity, relative humidity and visibility on IR atmospheric transmittance are examined. Predictions from LOWTRAN 5 for similar meteorological conditions are made and the corresponding data compared. A brief qualitative analysis is also reported on some scintillation data recorded during IR transmission measurements.

2. INSTRUMENTATION

The instrumentation used to measure absolute, broadband IR atmospheric transmittance and basic meteorological parameters has already been described in detail(ref.2,3). In brief, the transmission measuring equipment consists of a trailer-mounted broadband IR source and a van-mounted radiometer able to operate up to ranges of 10 km. The system can measure the absolute atmospheric transmittance in selected spectral regions using a combination of three cooled detectors (PbS, InSb and MCT) and spectral filters. The efficient IR source is a re-entrant conical black-body cavity with an aperture of 100 cm^2, a nominal surface temperature of 975 K and a total radiant power output of approximately 500 W. Both the IR source and radiometer are calibrated as described in reference 3. Appendix I gives the derivation of the transmissometer measurement equation while a summary of the error analysis performed on this system is given in Appendix II.

During the transmittance measurements the air temperature, relative humidity, visibility, sea state, wind speed and wind direction were monitored. Wet and dry temperatures, and aerosol extinction coefficient (at λ = 0.55 μm) were measured at the two ends of the transmission path at 10 min intervals and the data averaged.

Atmospheric particulate matter was sampled during measurements at the radiometer end of the path using

(i) 47 mm diameter Millipore filters with 0.1 μm pore size at flow rates of approximately 4.5 L/min and

(ii) 120 mm diameter Whatman 41 filters with flow rates of approximately 0.5 m^3/min.

Results from the analysis of these filters will be the subject of later reports. Briefly, the samples on the Millipore filters provided aerosol size distribution curves and the Whatman 41 samples were analysed using x-ray fluorescence techniques to determine the elemental composition of the aerosol, quantitatively.

3. SITE DESCRIPTION

The atmospheric transmittance and meteorological measurements were made at the same coastal site referred to in reference 2. This site was chosen as best suiting the requirements for open, ocean-type sea conditions, ie it has prevailing on-shore winds not passing immediately over continental land masses and has a low industrial contamination. Figure 1 shows the relative location of the site with respect to Adelaide, while figure 2 gives details of the two transmission paths used (5.03 and 9.05km) and the topography of the site.

4. DATA ANALYSIS

The data reported in this paper cover the period from October 1978 to December 1979. Transmittance measurements were made on 62 days during this period for 5.03 and 9.05 km pathlengths and in the spectral regions defined by the filter half power points listed in Table 1 below.

TABLE 1. BROADBAND SPECTRAL REGIONS SELECTED FOR ATMOSPHERIC TRANSMITTANCE MEASUREMENTS

Filter No.	Half Power Points (μm)	Filter No.	Half Power Points (μm)
1	1.480-2.500	8	4.410- 5.410
2	1.440-1.820	10	8.200-11.760
3	1.910-2.470	11	8.330- 9.800
5	3.550-4.000	12	10.470-10.700
7	4.360-4.590	13	0.955- 1.150

Figure 3 reproduces the spectral curves of the filters used.

All transmission and meteorological data were stored on a IBM 370/3033 computer and programmes were written to sort and plot the transmission data into the required parameter groupings. The transmittance data were derived from the recorded radiometer output signals which spanned at least a 3 min interval and which were averaged by eye. Measurements for each filter/detector combination were not made at regular intervals but generally repeated as soon as the filter wheel completed one revolution. (The maximum number of filters which could be held in the wheel at one time was seven). The radiometer data were converted using the appropriate calibration factors measured in the laboratory for each filter/detector combination used. Those data where there was an indication that precipitation possibly existed in the path were not included in the data set.

The data were sorted to show the variability of atmospheric transmittance with

(i) water vapour content for filters 5 to 12 and

(ii) visibility for filters 1,2,3,5 and 13.

Further subdivision of the data group related to water vapour content was not undertaken because of the limited range of air temperatures measured (13 to

23°C) and the insufficient number of data when smaller temperature intervals were chosen (see Section 5.1). The data related to visibility was further subdivided to accept only those readings associated with on-shore winds which at this site generally fell within SSW and ESE. Because only limited variations in wind speed (0.5 to 10 ms) and sea state conditions were experienced no division of the data was made with these parameters.

It is interesting to note that visibilities ($= 3.91/\sigma_{aerosol}$) as measured with integrating nephelometers at two locations along the sight line were greater than 50 km on those days measurements were made. This is not unexpected as the site is located where fogs and low maritime visibilities are not generally experienced. The temperature and absolute humidity were monitored for each end of the path and averaged as described in reference 2. The average wind angle over a particular hour was allocated one of eight 45° intervals while the corresponding average wind speed was assigned a Beaufort number. These classifications are summarised in Table 2.

TABLE 2. CLASSIFICATION OF WIND SPEED AND DIRECTION

Wind Classification No.	Wind Angle Interval (degrees)	Wind Speed Interval (ms)
1	338- 23	0.3- 1.5
2	23- 68	1.6- 3.3
3	68-113	3.4- 5.4
4	113-158	5.5- 7.9
5	158-203	8.0-10.7
6	203-248	10.8-13.8
7	248-293	13.9-17.1
8	293-338	17.2-20.7

Figures 4 and 5 reproduce plots of transmittance versus absolute humidity content covering all visibilities encountered for six spectral regions and two pathlengths studied. Transmittance data shown in the two figures were, however, grouped into four temperature intervals. Figures 6 to 8 reproduce plots of transmittance versus visibility where the data for each group has been divided into five relative humidity intervals.

In examining more closely the effects of water vapour content on transmittance a similar procedure was used as described in reference 2. Transmittance data for a particular spectral region and visibility grouping were divided into equal intervals of 0.5 gm/m^3 absolute humidity and the data falling within each interval averaged. Hence, in figures 9 to 11 and 13 to 15 the crosses represent the average values and the bars the extreme data limits whilst the number of data falling in each interval are given in the figure. The absolute humidity interval of 0.5 gm/m^3 was selected as it represents the maximum uncertainty likely to be experienced in the measurement of absolute humidity along the path.

For the detailed analysis of the effects of the maritime aerosol on transmittance in the 1.0 to 4.0 μm spectral region, the data for each range were grouped into equal visibility intervals of 20 km and five equal intervals of relative humidity between 45 and 95%. Data falling in each visibility and relative humidity interval were averaged and figures 19 to 26 reproduce these averaged data. The crosses represent the average values and the circles the extreme data limits. The contribution of the aerosol extinction coefficient to the total extinction coefficient in the 4.4 to 5.4 μm and 8 to 12 μm

spectral region is small compared to the molecular extinction for those visibilities experienced at the Victor Harbor site. The lower visibility of 50 km recorded at the site gives maritime aerosol extinction coefficients of approximately 0.020 km^{-1} and 0.014 km^{-1} for the two spectral regions at a 80% relative humidity, as compared with the measured lower limit of effective total extinction coefficients of 0.3 and 0.1 km^{-1}, respectively. For these reasons no plots of transmittance versus visibility are provided for these two regions and as well no distinction was made between off-shore and on-shore winds for the visibility groups in figures 9 to 15.

4.1 LOWTRAN 5 computations

The analysis has included the comparison of measured transmittance with the predicted values from LOWTRAN 5 for similar meteorological conditions. In this analysis the data have been presented in both the form of effective transmittance and effective extinction coefficients for a particular wavelength interval. The effective transmittance computations using LOWTRAN 5 were carried out by the numerical integration of the two integrals given in equation (I.5) in Appendix I; these data are represented by the solid lines labelled LT5 in the figures. Exceptions to this general rule are figures 14 and 15, where LT5A computations are represented by a solid line and LT5 computations by a dashed line. Plots of measured versus calculated effective extinction coefficients are also presented. These plots provide a possible means of determining the deviation of the slope of a least-squares fitted curve from the 1:1 situation; the fitted curves are represented by the dashed lines in figures 12 and 16. The contribution from the regression of the calculated extinction coefficients on the measured coefficients (coefficient of determination r^2) can also be computed. It should be pointed out that linear regression analysis is not strictly applicable when uncertainty in both sets of data is comparable but if caution is used in interpreting the results some indication of trends can be ascertained. (The LOWTRAN code has been derived to model low-resolution atmospheric transmittance to within 10%). It was further assumed that the fitted linear curve passed through the origin. This would be true if the calibration constants for each filter/detector combination were correct, and the trend of the data in the plots indicated that this was generally close to being the case, particularly in the 8 to 12 μm region where smaller extinction coefficients are experienced.

It should be noted that the effective extinction coefficient is the sum of the aerosol and effective molecular extinction coefficients. The effective molecular extinction coefficient is determined for a particular pathlength and wavelength interval $\Delta\lambda$. As many direct spectral absorption lines occurring within $\Delta\lambda$ are not resolved the Bouger exponential transmittance law $T_{eff} = \exp(-\sigma R)$ cannot generally be used. This arises because the fine structure of the spectrum varies differently with pathlength as a result of selective absorption, and thus the effective molecular extinction coefficient cannot be used to compute the molecular atmospheric transmittance for other pathlengths and wavelength intervals. The aerosol extinction coefficient, however, only varies slowly with wavelength and does obey the exponential transmittance law.

5. RESULTS AND DISCUSSION

This section will describe the results of the analysis of variation of transmittance with absolute humidity and visibility. One general comment can be made about the scatter that is always evident when atmospheric transmittance measurements are made. It is readily apparent that the scatter

in the reduced transmittance data for the October 1978 to December 1979 period is less than the scatter in the corresponding data measured between November 1977 and April 1978 and reported in reference 2. During a laboratory calibration carried out between these two periods it was found that the alignment of the detectors in the radiometer was not correct and this appeared to have resulted in signals from the source not always being correctly peaked.

5.1 Variation of atmospheric transmittance in the 8 to 12 μm region

In this section the results obtained with filters 10,11 and 12 are discussed. The meteorological parameter which has most influence on atmospheric transmittance in this spectral region is the absolute humidity or the water vapour content in the path. Although this region does not contain many strong spectral absorption lines arising from the uniform gas mixture and water vapour, there is a strong anomalous absorption which varies only slowly with wavelength, and which dominates the transmittance. Modelling of this anomalous absorption by water vapour in LOWTRAN 5 is based on an expression for water continuum absorption derived empirically from laboratory measurements on water vapour absorption in short pathlength cells. This expression, summarised in reference 4, exhibits a quadratic dependence on water vapour pressure. However, the fundamental form this molecular absorption mechanism takes is still subject to conjecture, and currently two theories exist about the mechanisms involved(ref.5,6). Laboratory and field measurements to date have indicated that the empirical model used in LOWTRAN 5 predicts the extinction coefficient for anomalous water vapour absorption to a reasonable degree of accuracy for water vapour content up to 15 gm/m^3 for air temperatures in the region of 20 to 25°C. There is not sufficient data with a wide spread of temperature to check with accuracy, the negative temperature (exponential Boltzmann-like) dependence of the form exp{A(296/T-1)} that this anomalous absorption was been predicted to follow.

The transmittance data obtained from the Victor Harbor site are reproduced in figures 4(a), 4(b) and 4(c) as plots against absolute humidity. In these plots, the transmittance data were further subdivided into temperature intervals of 5°C. It is evident that most of the data are associated with air temperatures ranging from 13 to 23°C. In view of the small temperature range and the small number of data falling into a given temperature and absolute humidity interval, it was decided not to perform any analysis with temperature as a parameter. Computations undertaken with the current version of LOWTRAN provide transmittance values that change by a maximum value of 0.04 transmittance at the maximum measured absolute humidity of 15 gm/m^3 in the temperature range 13 to 23°C. Hence, it would be unlikely such changes in transmittance with temperature could be detected in the present data unless a large number of measurements were taken to reduce to a minimum, the scatter in transmittance.

The plots of averaged transmittance data for each equal absolute humidity interval (figures 9 to 11) indicate reasonable agreement with LOWTRAN 5 predictions. To quantify these differences, plots of calculated versus measured effective extinction coefficient (refer to Section 4.1) were done. Figures 12(a), 12(b) and 12(c) reproduce those plots where the aerosol extinction coefficient was less than 0.04 km^{-1}. This figure was chosen because most of the visibilities occurred in this region and since the aerosol extinction coefficient is small (even for relative humidities around 80%) it would only contribute a small uncertainty to the transmittance. The results of the linear regression analysis are summarised in Table 3.

The values of b, the slope of the regression line, indicate that the

TABLE 3. SUMMARY OF LINEAR REGRESSION ANALYSIS FOR THE 8 TO 12 μm SPECTRAL REGION

(a) Visibility < 96 km

Filter No.	Spectral Region (μm)	Range							
		5.03 km				9.05 km			
		b	r^2	SD	Uncertainty in T_{eff}	b	r^2	SD	Uncertainty in T_{eff}
10	8.20-11.76	1.12	0.997	0.009	+0.05 -0.09	1.12	0.975	0.028	+0.20 -0.12
11	8.33- 9.80	0.977	0.995	0.012	±0.06	1.03	0.975	0.026	+0.18 -0.11
12	10.47-10.70	0.921	0.993	0.015	+0.08 -0.07	1.07	0.974	0.029	+0.21 -0.12

(b) Visibility > 96 km

Filter No.	Spectral Region (μm)	Range							
		5.03 km				9.05 km			
		b	r^2	SD	Uncertainty in T_{eff}	b	r^2	SD	Uncertainty in T_{eff}
10	8.20-11.76	1.20	0.997	0.01	+0.06 -0.04	1.13	0.992	0.015	+0.09 -0.07
11	8.33- 9.80	1.12	0.982	0.02	+0.12 -0.08	1.05	0.995	0.011	±0.06
12	10.47-10.70	0.999	0.985	0.02	+0.12 -0.08	1.09	0.983	0.02	+0.12 -0.09

average fit of the calculated data to the measured data is within 13% except for one filter/range combination. Assuming an uncertainty of plus or minus two standard deviations between the calculated and measured extinctions and assuming mean transmittances of 0.5 and 0.3 for the two ranges 5.03 and 9.05 km respectively, then the uncertainty in the effective extinction coefficient can be translated to an uncertainty in the transmittance. The values listed in Table 3 reveal a reasonably consistent uncertainty in transmittance for the 5.03 km range while there appears to be a higher uncertainty for the 9.05 km range.

5.2 Variation of atmospheric transmittance in the 3.5 to 5.5 μm region

The results discussed in this section cover the data obtained for filters 5,7 and 8 (see figures 5(a), 5(b) and 5(c)). The main meteorological parameter influencing the transmittance is again water vapour with maritime aerosol extinction also contributing but to a lesser extent. This region is characterised by strong absorption due to the many spectral absorption lines arising from H_2O and CO_2 molecules as well as a N_2 continuum absorption, and an anomalous absorption due to water vapour continuum.

5.2.1 4.4 to 5.4 μm spectral region

Referring to previous investigations by this author in the 4.4 to 5.4 μm spectral region(ref.4) it was found that the addition of water vapour continuum absorption to the LOWTRAN model improved considerably the accuracy of the predictions. Ben-Shalom et al in a recent paper(ref.7) also reported spectral transmittance measurements with a resolution of 0.07 μm for the 4.3 to 5.5 μm region which showed a similar discrepancy when compared with computed transmittances from LOWTRAN 4. After they included the water continuum absorption expression into LOWTRAN, as suggested by this author(ref.4), good agreement is obtained for pathlengths near 6 km although it is not clear whether they extended the water continuum absorption expression down to 4.3 μm. Their experimental measurements(ref.8) also provided values of the self-broadening absorption coefficient in the water continuum absorption expression which were in agreement (to within about 50%) with those derived by this author. Considering the various experimental errors involved, this agreement is encouraging.

However the transmittance data reported here for the 4.4 to 5.4 μm region (figures 14 and 15) indicate that the measured effective transmittance is lower than that given by calculation using LOWTRAN 5 (see LT5 curves in the figures) and the discrepancies are dependent on pathlength and absolute humidity. It would appear that the water continuum absorption model included in LOWTRAN 5 may not account completely for the discrepancies observed in this spectral region.

Recently(ref.9) AFGL have examined this region and computed curves for self and foreign broadening absorption coefficients ($C_s(\nu,T)$ and $C_F(\nu,T)$) over the region from ν=100 to 3000 cm^{-1} due to far wing absorption of H_2O absorption lines. These curves have been used to compute the water continuum transmittance curve in figure 17(a) for the conditions stated, over 1800 to 3000 cm^{-1} region. Also included are the transmittance curves derived from the water continuum absorption coefficients used in LOWTRAN 5 for 2400 to 3000 cm^{-1} region, and by the author for the 2000 to 2200 cm^{-1} region. In view that the data in the 2000 to 2200 cm^{-1} region were derived from field measurements the agreement is reasonable. Figure 17(b) shows a plot of $\gamma = C_s/C_F$ versus ν derived from the calculated $C_s(\nu,T)$ and $C_F(\nu,T)$ in reference 9. It is noted that γ varies over the range of 0.02 to 0.12 and it is clearly evident that water continuum calculations for this region should include γ as a function of ν. (LOWTRAN 5 assumes a fixed value of 0.12 for the 2400 to 3000 cm^{-1} region.) In figures 14 and 15 the LT5 curves refer to computed curves using LOWTRAN 5, and LT5A curves to LOWTRAN 5 incorporating the AFGL water continuum absorption data over 1800 to 3000 cm^{-1} region and γ varying with wavelength as in figure 17(b). The maritime aerosol model was used for all LOWTRAN computations.

In the case of filter 8 the agreement of the data are reasonable while for filter 7 there appears to be evidence of a significant discrepancy remaining. In order to quantify the differences between the measured and calculated data using the new continuum data, a linear regression analysis was performed on the calculated and measured effective extinction coefficients for filters 5, 7 and 8. (Plots of these data

TABLE 4. SUMMARY OF LINEAR REGRESSION ANALYSIS FOR THE 3.5 TO 5.5 μm REGION

(a) Visibility <96 km

Filter No.	Spectral Region(μm)	Range					
		5.03 km			9.05 km		
		b	r^2	SD	b	r^2	SD
5	3.55-4.00	0.74	0.978	0.015	0.71	0.992	0.007
7	4.36-4.59	0.84	00.998	0.018	0.83	0.999	0.005
8	4.41-5.41	0.965	0.998	0.018	0.93	0.999	0.005

(b) Visibility >96 km

Filter No.	Spectral Region(μm)	Range					
		5.03 km			9.05 km		
		b	r^2	SD	b	r^2	SD
5	3.55-4.00	0.95	0.950	0.018	0.86	0.996	0.005
7	4.36-4.59	0.89	0.998	0.019	0.81	0.995	0.010
8	4.41-5.41	1.04	0.997	0.020	0.93	0.995	0.012

NB: Effective extinction coefficients calculated with new AFGL water continuum absorption data(ref.9)

for the high visibility groups are shown in figures 1a(b) and 1c(b). In all except one case the slope b of the fitted curves all were less than 1.0 (see Table 4).

Because filter 7 has a narrow bandpass, errors may arise from the filter's spectral curve which could introduce a small constant error into the calibration constants and, combined with low transmittance values, cause the discrepancy observed in figure 1a. Hence, the differences in computed and measured transmittance for the 4.4 to 4.6 μm region were examined more closely. The transmittance data in figure 1a were fitted with linear curves using linear regression analysis and the difference in the calculated and measured effective extinction coefficients determined for a given absolute humidity. The results are given in Table 5. Three out of the four sets of data exhibit a near constant difference with water vapour in support of the argument that a constant error may explain the discrepancy. (It is pointed out that the computed transmittance values using filter 7 reported in reference 2 are in error since transmittance was calculated between wavelengths corresponding to the filter half power points and not for wavelengths covering the whole filter spectral range as now done). Any discrepancy arising in the LOWTRAN computation of the spectral absorption due to the band model used for the uniformly mixed gases has been ruled out following checks in this region with the 1978 AFGL atmospheric line compilation tape HITRAN(ref.2).

TABLE 5. ESTIMATED DISCREPANCY IN CALCULATED AND MEASURED EFFECTIVE EXTINCTION COEFFICIENTS AS A FUNCTION OF ABSOLUTE HUMIDITY FOR 4.4 TO 4.6 μm REGION

(a) Visibility <96 km

Range (km)	Absolute humidity (gm/m^3)		
	6	9	12
5.03	0.072 km^{-1}	0.077 km^{-1}	0.077 km^{-1}
9.05	0.053	0.064	0.061

(b) Visibility >96 km

Range (km)	Absolute humidity ($gm\ m^3$)		
	6	9	12
5.03	0.036 km^{-1}	0.048 km^{-1}	0.058 km^{-1}
9.05	0.030	0.061	0.134

5.2.2 3.5 to 4.2 μm spectral region

For the transmittance data measured in the 3.55 to 4.[illegible] μm region linear regression analysis reveals a greater variability in the slope of the fitted curves (see Table 4 and figure 10(a)). Some of this variation must arise from experimental errors when transmittance values are high (see Appendix II). For water vapour concentrations up to about 12 gm/m^3, the Haught and Cordray and Ben-Shalom et al spectral transmittance data(refs.7,10 and 11) measured over 5 to 6 km pathlengths have shown reasonable agreement with LOWTRAN 5. There is evidence, however, of a discrepancy in both groups of data when water vapour concentrations exceed 12 gm/m^3. In reference 4 it was reported that there existed a discrepancy between laboratory measurements of the 3.5 to 4.0μm H_2O continuum absorption coefficients at 296 K by White et al(ref.12) and Burch et al(ref.13).

More recently, Watkins et al(ref.14) carried out further laboratory measurements (using the Atmospheric Sciences Laboratory 21 m absorption cell) to determine more precisely the nature of the continuum absorption at ambient temperatures. Their results indicated that there are contributions from both far wing and aggregate water molecule (eg water dimer or ion cluster) types of absorption. In contrast the Burch data for 296 K (on which the continuum absorption model used in LOWTRAN is based) are derived by extrapolation from data measured at 338 K where apparently the predominate absorption is due only to the far wing type, ie the LOWTRAN model under-estimates the transmittance because of the missing aggregate water molecule type of absorption. The inclusion of this type of absorption makes the overall continuum absorption more strongly dependent on water vapour pressure than is presently shown by the model in LOWTRAN. As a result of the reduced dependence of the water vapour continuum absorption on foreign pressure broadening the absorption will not fall off as rapidly with combined

N_2-O_2 pressure (eg with increasing altitude as is the case with the present model). As the two types of absorption contribute approximately equal proportions at 24°C the continuum extinction coefficients are now double those given by the model in LOWTRAN.

To see whether this new model will go some way to accounting for the discrepancy reported in the overseas data measured at high water vapour pressures an illustrative example is provided. The data from Table 6 of Watkins et al for 80% relative humidity (which corresponds to 17.25 gm/m^3 at 24°C) were used to compute a correction factor at selected wavelengths to the continuum absorption data used in LOWTRAN. These factors were applied to the 5.1 km pathlength LOWTRAN curve given in figure 1(c) of Haught and Cordray. The modified LOWTRAN data points are reproduced in figure 18 along with the spectral transmittance curve originally measured by Haught and Cordray. As no mention is made of the temperature at which the original LOWTRAN computations were made, the temperature of 24°C had to be used. Except for the 2700 to 2800 cm^{-1} (3.70 to 3.57 μm) region the transmittance predictions of the modified LOWTRAN model are closer to the measured values.

The discrepancy in the 2700 to 2800 cm^{-1} region is not supported by the H_2O continuum transmittance data in figure 17(a) based on the new AFGL computed continuum absorption data. Data given in that figure for 2600 to 2700 cm^{-1} region does indicate about a 0.93 correction factor needs to be applied to the present LOWTRAN 5 H_2O data.

Furthermore, the temperature dependence of the H_2O continuum absorption for this spectral region requires more laboratory investigations to define the precise relationship. The Watkins et al H_2O continuum model predicts that the absorption will show a much stronger dependence on temperature near 20°C than the Burch data now presently used in LOWTRAN. Also insufficient field data on transmittance exists in this region to examine the temperature dependence of H_2O absorption. The present data are limited in number and too largely scattered for doing any analysis of transmittance variability with temperature.

It is interesting to note that Haught and Cordray derived an alternative algorithm by fitting a polynomial to their data for this spectral region. This algorithm did give a better fit to their data at high water vapour pressures but takes no account of ambient temperature which varied over 5°C to 30°C. Caution is necessary in the use of algorithms which are based purely on field measurements; they should only be used for conditions under which the measurements are made and not over the large range of conditions generally experienced in the atmosphere for which they have not been tested.

Figure 19 shows plots of effective transmittance data versus visibility within selected relative humidity intervals for the 3.55 to 4.00 μm region. Because of the low aerosol extinction coefficients measured, agreement can be considered to be reasonable. Recently data have been reported(ref.15) in which LOWTRAN 3B maritime aerosol extinction coefficients calculated at 3.75 μm within the mixed layers agree, to within a factor of 1.5 to 2, with the coefficient calculated using actual measured aerosol size distributions when measured visibilities were of the order of 10 to 23 km. (LOWTRAN 3B aerosol extinction coefficients were computed for a fixed RH of 80%).

To summarise for this region, the model for H_2O continuum presently used in LOWTRAN 5 will need replacing by a two component model once the temperature dependence of the absorption has been determined. Broadband transmission measurements planned for the tropical environment using the present equipment will provide field data needed for verification of updated models for water vapour concentrations falling within 15 to 25 gm/m^3.

5.3 Variation of atmospheric transmittance in the 1.0 to 2.5 μm region

In this spectral region atmospheric transmittance variations are much more influenced by atmospheric aerosol absorption variations than water vapour absorption variations. Water vapour absorption is confined to spectral line absorption with evidence that there is very little water vapour continuum absorption. Analysis of the data in this region has been confined to examining the effects of aerosol absorption on transmittance which is in turn a function of aerosol number density, size distribution, type of aerosol and the relative humidity. Data for this region were divided into onshore and offshore wind groups and plotted as a function of visibility in four relative humidity groups. Figures 20 to 25 reproduce the data measured with filters 1,2,3 and 13 over the two ranges, 5.03 and 9.05 km, for onshore winds. The LOWTRAN 5 curve in each plot has been determined using the maritime aerosol model for a relative humidity selected at mid-range in the interval shown. The temperature was fixed at 17.5°C and the visibility measured at the time was used as an input to the LOWTRAN 5 model.

For the shorter range of 5.03 km (figures 20 to 23) a bias is evident whereby the measured values of transmittance tend to be below the predicted values for all values of relative humidity. Some of this difference no doubt can be accounted for by the low flow rate used in visibility meters allowing heating of the aerosol, and thereby reducing the effective humidity and size of the aerosol particles. Thus, visibilities actually recorded under these conditions were higher than were actually prevailing at the time.

Finally figure 26 provides an example of the transmittance data measured with filter 1 over the 5.03 km range for offshore winds. In this case the rural aerosol model in LOWTRAN 5 was used to compute the curves and it is evident that discrepancies exist. It is interesting to note that more data were recorded for the higher visibilities. For the same reasons given above, the aerosol extintion coefficient has probably been underestimated and this could account for some of the discrepancy seen.

5.4 Scintillation effects on incoherent IR transmitted radiation

5.4.1 Introduction

In this section only a brief descriptive review will be given of the effects of clear air turbulence on incoherent propagating beams. The reader is referred to more extensive coverages of the theory in references 16 and 17.

Radiation propagating through the atmosphere is not only attenuated by absorption and scattering but is also refracted and diffracted by refractive-index fluctuations due to small scale variations in air temperature. The resulting fluctuations in intensity of the transmitted radiation are known as scintillations. The size of the turbulent eddies present in the atmosphere is very important. Those eddies that are large compared with the receiver diameter tend to deflect the beam while

eddies small with respect to the receiver diameter diffract the radiation and cause scintillation. In general, a combination of these two effects prevails when long recording times are considered.

For the visible wavelengths the source of scintillation is known to be small scale fluctuations in the real component of the refractive index (which is responsible for dispersion of the wave front) caused almost exclusively by temperature fluctuations. However, scintillation of visible light can also be affected by strong humidity fluctuations which also affect the refractive index. These fluctuations in refractive index are expressed in terms of the refractive index structure constant C_N^2. Scintillation is strongest for near-horizontal paths that are close to the earth's surface ($C_N^2 \sim 10^{-14}$ $m^{2/3}$).

The instantaneous random pattern of scintillations, observed in a plane parallel to the wavefront, displays spatial Fourier components with a variety of scales. The predominant scale size is the Fresnel-zone size, $\sqrt{\lambda R}$. Thus for pathlengths of 10 km the predominant scale size varies between 10 and 32 cm for the IR wavelengths 1 and 10 μm, respectively. Now if a receiving aperture less than some critical size (eg $\sim \sqrt{\lambda R}$) exists such that the intensity fluctuations are correlated over its area, then the aperture will behave as a point detector. As the aperture size increases the intensity fluctuations become uncorrelated over the aperture and the intensity is a spatial average over some finite region of space, and the fluctuations tend to decrease. This effect is known as "aperture averaging".

5.4.2 Scintillation of infrared radiation

The diffraction theory has been moderately successful in predicting the magnitude of visible scintillations although saturation effects have not been so easily explained. However, there appears to be a scarcity of scintillation data for propagating incoherent IR beams, particularly involving large transmitted beams and receiving apertures as used in the present equipment. For IR wavelengths the scintillations should decrease for increasing wavelength (in fact by a factor of 27 from λ=0.63 to 10.6 μm) if they arise predominately from refractive index fluctuations. For large receiving apertures, these scintillations will be "aperture smoothed" thus further reducing their magnitude.

However, for the IR region one has also to examine the effects of absorption fluctuations arising from water vapour pressure and atmospheric pressure fluctuations. (The imaginary part of the refractive index and the absorption coefficient due to a single absorption line are related by the expression $\beta = 4\pi\nu n_I$ where ν is the wave frequency). A recent theoretical study(ref.18) has shown that

(i) for strong humidity fluctuations the refractive index fluctuations dominate in the IR and

(ii) absorption fluctuations contribute far less to the variance of log-intensity than the refractive fluctuations do.

Thus, for a point receiver one would still expect to have a smaller variance than in the visible region except in water bands where absorption is large and pathlengths are short.

This now raises the question with large receiving apertures; if

"aperture averaging" reduces the effects of refraction fluctuations will absorption fluctuations dominate? This, in effect, is saying that the variance of the log-intensity arising from absorption fluctuations is relatively unaffected by aperture size. This is a question about which little is known because of the limited experimental data available.

During the measurement of atmospheric transmittance at the Victor Harbor site, transmission signals recorded for wavelength regions between 1 and 12 μm (see Table 1) generally exhibited scintillation effects of varying magnitude. Earlier observations of scintillations during transmission measurements over land were briefly reported in reference 2 and indicated the frequencies of the scintillations fell within 10 to 15 Hz. In view of the above discussion and the large receiver aperture diameter (150 mm) with respect to the Fresnel-zone scale (which must imply some "aperture averaging"), scintillations of such magnitudes appear to arise from absorption fluctuations which could be due predominately to humidity fluctuations. It should be noted that the scintillations observed on the recorded transmission signals do not totally reflect the magnitude and frequencies of the scintillations. This arises from the fact that the phase sensitive detector is a highly selective filter for frequencies away from the fundamental chopping frequency (~195 Hz) and the integrator has a long time constant (~1 s). Hence, the recorded scintillation data can only be used for a relative analysis, that is, comparing scintillation behaviour within one or more measurement periods. As a general observation one can say that the magnitude of the scintillation does vary substantially from day to day. Table 6 lists measured relative fluctuations in the 1.48 to 2.50 μm, 3.55 to 4.0 μm and 8.20 to 11.76 μm regions over a 5.03 km path for scintillations observed between October and December 1979. Typically the magnitude has varied by a factor of 4 on different days. Variations in the relative peak fluctuations

$$= \frac{\text{Peak-to-Peak Fluctuation} \times 100}{\text{Average Signal}} \ (\%)$$

over a measurement period on a particular day were fairly similar for the three regions (except for 2/10/79) which appears to indicate that the fluctuations are not sensitive to wavelength. If any dependence does exist, the relative fluctuations appear to be slightly less for the 1.48 to 2.50 μm region. On all but three of the days in Table 6 both the mean temperature and the absolute humidity varied little over the measuring period. Thus absorption fluctuations must have been responsible for the greater part of the signal fluctuations since "aperture averaging" is expected to minimise real refractive index fluctuations.

These conclusions are substantiated by two further observations. Firstly measurements(ref.19) have shown that the temperature structure parameter C_T^2 and hence the refractive index structure coefficient C_N^2 varies approximately with height Z above the water surface according to $Z^{-4/3}$ and $Z^{-3/2}$ for unstable and stable conditions respectively. At Victor Harbor the path height varies over the water from about 3 to 20 m which would imply a fall in C_T^2 by a factor of 0.24 for the heights involved in the unstable situations which were expected to prevail at the time the measurements were made. Secondly, signal fluctuations did

TABLE 6. RELATIVE SIGNAL FLUCTUATIONS MEASURED OVER 5 km PATHLENGTH FOR 3 SPECTRAL REGIONS BETWEEN OCTOBER AND DECEMBER 1979

Date	1.48 to 2.50 μm		3.55 to 4.00 μm		8.20 to 11.76 μm	
	Local Time	Relative Fluctuation (%)	Local Time	Relative Fluctuation (%)	Local Time	Relative Fluctuation (%)
2/10/79	1324	3.5	1415	50.0	1333	6.5
	1438	7.0	1530	50.0	1450	6.5
	1557	7.0	1654	50.0	1610	7.0
	1714	3.5			1721	10.5
3/10/79	1055	2.5	1137	5.0	1109	6.0
	1205	4.0	1245	9.0	1218	6.0
	1314	3.0			1319	6.0
11/10/79	1321	2.5	1411	2.5	1718	5.0
12/10/79	1112	4.5	1148	9.5	1122	8.0
	1335	11.0	1307	10.0	1331	16.0
25/10/79	1305	4.0	1352	5.0	1324	5.0
	1423	3.0	1509	5.0	1439	5.0
	1534	4.0	1609	4.7	1545	5.0
31/10/79*	1324	13.0	1411	18 0	1339	14.0
	1450	7.5	1536	19.0	1504	6.5
	1608	4.0	1712	4.0	1624	5.0
	1746	4.0	1837	9.5	1800	3.5
	1904	10.0	2001	9.0	1924	10.0
1/11/79	1531	7.5	1619	9.0	1544	10.5
	1636	5.0	1746	8.5	1711	10.0
	1816	5.0			1828	8.0
7/11/79	1324	7.0	1413	7.5	1338	8.0
	1446	7.0	1535	9.5	1500	9.0
	1608	7.0	1704	7.5	1623	9.0
	1736	5.5	1825	5.0	1749	7.0
	1857	4.5	1945	5.5	1911	6.5
12/11/79	1316	7.5	1403	7.5	1330	7.0
	1436	7.5	1519	8.0	1448	8.5
	1551	6.0	1635	8.5	1604	8.5
	1711	7.5	1759	8.5	1725	9.5
	1831	6.5	1919	8.5	1845	9.0
28/11/79	1324	8.0	1409	8.0	1336	9.0
	1447	5.0	1537	6.5	1503	8.5
	1610	6.5	1701	8.3	1623	10.5
	1731	4.0	1815	8.0	1743	10.0
	1852	4.0	1940	6.0	1907	9.5
4/12/79*	1328	14.0	1415	14.0	1342	12.0
	1449		1539	4.0	1504	3.0
	1610	2.5	1648	3.5	1622	4.0
	1740	2.0	1824	6.0	1752	7.0
	1856	4.0	1939	4.5	1910	6.0
6/12/79	1100	9.0	1144	6.0	1112	9.0
	1218	4.5	1305	6.5	1232	8.0

* Refer to figures 27 and 28 for actual signal recordings.

not appear to change near sunset when the atmosphere generally can be expected to change from unstable (free convection regime) to stable conditions. In earlier measurements performed about 2 m above the ground, signal fluctuations did show evidence of falling as sunset was approached.

It is also noteworthy to recall that in this period unusual scintillation behaviour was observed on three different days. On 31/10/79 and 4/12/79 cold fronts passed over the Victor Harbor site while measurements were being made which resulted in a sharp drop in temperature and an increase in absolute humidity. Figures 27 and 28 show the variation of temperature and absolute humidity as the cold fronts traversed the site. Actual transmission signals recorded for six minutes at the times indicated show a large change in the relative fluctuation as the absolute humidity increases and temperature decreases, simultaneously. In figure 28 the fast drop in signal fluctuations for 1.48 to 2.50 μm region at 1447 hours occurred as the front arrived at the site. During both these measurement periods, the sun was shining.

One possible explanation for this phenomena is that the approach of a cold front has reduced the air temperature to a value which is close to the surface temperature of the sea water. If this were to occur it is expected that temperature gradients near the surface would be small and combined with a well mixed air mass, the effect of the humidity fluctuations on log-intensity variance could be substantially reduced.

6. CONCLUSIONS

The Victor Harbor measurement site has provided data on IR transmittance for a coastal site in a temperate environment which was chosen because the onshore winds are expected to provide air masses which closely represent an open-ocean maritime environment. These data have been classified into spectral regions and various meteorological groups for analysis. The main analyses reported have been concerned with the comparisons of the transmittance data with LOWTRAN 5 predictions for similar meteorological conditions. It has been found that the data measured at the site still exhibit a degree of scatter which is larger than one would like and this, in part, can only be overcome by collecting a large amount of data for the wide range of meteorological conditions that can prevail.

The measured transmittance data were compared with the LOWTRAN 5 values in ten spectral regions. The comparisons made in the three spectral regions within the 8 to 12 μm region have shown reasonable agreement for absolute humidities up to 12 gm/m^3, where the temperature range was restricted and visibilities were high. This conclusion is supported by the data measured by G. Matthews et al at San Nicolas Island off the West coast of the USA (private communication). For those spectral regions studied in the 3 to 5.5 μm region the conclusions are different. The discrepancy which was reported previously in the 4.4 to 5.5 μm region was found to remain. Evidence now shows that this arises from the absence of water continuum absorption in the model for this region. The inclusion of a water continuum absorption component derived by AFGL into the LOWTRAN 5 computer code has improved the agreement although some discrepancy still remained for the 4.4 to 4.6 μm region. This could be due in part to errors in calibrating the system for a narrow spectral region and in determining very low transmittances for this region. The comparisons made in the 3.5 to 4.0 μm region showed more variability, probably arising from scatter in the data which is generally more than in the other spectral regions studied. Considering the accuracy of the data, the agreement is reasonable.

On the other hand results for the 1 to 2.5 μm region showed a greater variability. In this region the errors are greater. In addition to calibration errors, there are errors from (1) measuring visibilities and (2) using a rather simple growth model aerosol in LOWTRAN 5 to predict the effects of high humidities on extinction by the maritime aerosol. No attempt was made to factor out the aerosol component that contributes to the total effective extinction coefficient. This calculation would rely on the accuracy of the LOWTRAN 5 model to predict the molecular extinction coefficient for given meteorological and range conditions. As far as is known however, the molecular spectral absorption data for the 1 to 2.5 μm region is reasonably accurate. Even so this calculation must still introduce some uncertainty which would be difficult to estimate accurately. Considerably more data will need to be obtained in this region to check the influence of maritime aerosol on extinction during high humidities.

The observations reported here on IR scintillations reveal that a significant level of scintillation from 1 to 12 μm is superimposed on the transmission signals received by the radiometer. In a strictly relative comparison, there does not appear to be any strong dependence on wavelength, and the scintillations are not directly attributable to variations in the real refractive index arising from temperature fluctuations. It is highly probable that the scintillations observed are due to fluctuations in the imaginary component of the refractive index resulting from humidity fluctuations in the atmosphere. It would appear that if the air mass is extremely well mixed (as occurs with cold fronts), the scintillations are considerably reduced.

7. FUTURE WORK

A further measurement programme has been initiated to gather more data on IR transmittance at a coastal site, this time in the tropical environment which is predominately characterised by high water vapour densities (up to 25 gm/m^3) and high relative humdities (>90%). Data are particularly required on the influence of water continuum absorption at high water vapour densities, as little experimental data are available to compare model predictions in the 3 to 5 and 8 to 12 μm regions. In the case of high humidities the extinction due to the maritime aerosol (which is mainly composed of sea-salt) is significantly increased due to the growth of such particles. A laser extinction measuring system will provide absolute transmittance data at 0.55 and 1.06 μm wavelengths and provided accurate measurements of relative humidity above 90% can be made, transmittance data at these two wavelengths can be measured as a function of this variable. Such data will be valuable in verifying and updating models used to predict the effects of relative humidity on maritime aerosol extinction.

NOTATION

β	absorption coefficient
γ	ratio of self to foreign broadening absorption coefficients
ε'	emissivity of field black-body source
ε	emissivity of calibration black-body source
λ	wavelength (μm)
ν	wavenumber (cm^{-1})
π	3.1416
σ_{eff}	effective extinction coefficient
b	slope of regression line
e_T	resultant external error estimate
n_I	imaginary component of refractive index
r^2	coefficient of determination
$w'(\lambda,T)$	radiant flux/unit area of field black-body source at temperature T
$w(\lambda,T)$	radiant flux/unit area of calibration black-body at temperature T
A_i	area of calibration black-body source aperture
A_R	area of receiver aperture
A_s	area of field black-body source aperture
$C_s(N,T)$	self broadening absorption coefficient
$C_F(\nu,T)$	foreign broadening absorption coefficient
C_N^2	refractive index structure parameter
C_T^2	temperature structure parameter
D_s	diameter of field black-body source aperture
E_T	total lower bound of relative error (%)
E_{Tmax}	total upper bound of relative error (%)
F	focal length of collimator mirror
G	receiver amplifier gain factor
$J'_{\Delta\lambda}$	source radiant intensity (w/sr)
K	constant

R	pathlength (km)
$R(\lambda)$	detector spectral response
$R_{\Delta\lambda}$	receiver responsivity measured by linear regression analysis
$R^1_{\Delta\lambda}$	receiver responsivity over wavelength interval $\Delta\lambda$(V/W)
R_M	collimator mirror reflectance
T	temperature (K)
$T(\lambda,R)$	atmospheric spectral transmittance
T_{ave}	average atmospheric transmittance
T_{eff}	effective average atmospheric transmittance
T_F	receiver filter spectral transmittance
V	receiver output voltage
V_i	receiver output voltage for calibration source aperture area A_i
$W^1_{\Delta\lambda}$	integrated radiant flux/unit area from field source
$W_{\Delta\lambda}$	integrated radiant flux/unit area from calibration source

REFERENCES

No.	Author	Title
1	Kneizys, F.X. et al	"Atmospheric Transmittance/Radiance: Computer Code LOWTRAN 5". AFGL-TR-80-0067, February 1980
2	Cutten, D.R.	"Preliminary Assessment of Infrared Transmission Data Measured Over 'Ocean-Type' Waters in a Temperate Environment". ERL-Technical Memorandum 0063-TM, 1979
3	Cutten, D.R.	"Instrumentation for Investigating the Propagation of Infrared Radiation Over Long Atmospheric Paths". WRE-Technical Report 1889(A), 1978
4	Cutten, D.R.	"Extension of Water Vapour Continuum Absorption to the 4.5 to 5.0 μm Region". Infrared Physics, Vol.19, Page 665, 1979
5	Burch, D.E. and Gryvnak, D.A.	"Laboratory Measurements of the Infrared Absorption by H_2O and CO_2 in Regions of Weak Absorption". Proceedings Society Photo-optical Instrumentation Engineers (Optical Properties of the Atmosphere) Vol.142, page 16, 1978
6	Suck, S.H. et al	"Water Cluster Interpretation of IR Absorption Spectra in the 8 to 12 μm Wavelength Region". Applied Optics, Vol.18, page 2609, 1979
7	Ben-Shalom, A. et al	"Long Path High-Resolution Atmospheric Transmission Measurements: Comparison With LOWTRAN 3B Predictions: Comments". Applied Optics, Vol.20, page 171, 1981
8	Ben-Shalom, A. et al	"Absorption by Atmospheric Water Vapour in the Region 4.2 to 5.5 μm". Proc. Int. Rad. Symp. Fort Collins Colorado, August 1980, page 219
9	Clough, S.A. et al	"Atmospheric Spectral Transmittance and Radiance: FASCOD1B". Proceedings Society Photo-optical Instrumentation Engineers, April 20-24, 1981 (In print)
10	Haught, K.M. and Cordray, D.M.	"Long Path High-Resolution Atmospheric Transmission Measurements: Comparison With LOWTRAN 3B Predictions". Applied Optics, Vol.17, page 2668, 1978

No.	Author	Title
11	Ben-Shalom, A. et al	"Spectral Characteristics of Infra-Red Transmittance of the Atmosphere in the Region 2.8 to 14 μm - Preliminary Measurements". Infrared Physics, Vol.20, page 165, 1980
12	White, O. et al	"Water Vapour Continuum Absorption in the 3.5 to 4.0 μm Region". Applied Optics, Vol.17, page 2711, 1978
13	Burch, D.E., Gryvnak, D.A. and Pembrook, J.D.	"Investigation of the Absorption of Infrared Radiation by Atmospheric Gases: Water, Nitrogen, Nitrous Oxide". Philco-Ford Aeronatronic Division Report U-4784, (AFCRL-71-0124), January 1974
14	Watkins, W.R. et al	"Pressure Dependence of the Water Vapor Continuum Absorption in the 3.5 to 4.0 μm Region". Applied Optics, Vol.18, page 1149, 1979
15	Hughes, H.G.	"Aerosol Extinction Coefficient Variations with Altitude at 3.75 μm in a Coastal Marine Environment". J. Applied Meteorology, Vol.19, page 803, 1980
16	Lawrence, R.S. and Strohbehn, J.W.	"A Survey of Clear-Air Propagation Effects Relevant to Optical Communications". Proceedings IEEE, Vol.58, page 1523, 1970
17	Tatarskii, V.I.	"Wave Propagation in a Turbulent Medium". McGraw-Hill Book Co., New York, 1961
18	Hill, R.J. Clifford, S.F. and Lawrence, R.S.	"Refractive Index and Absorption Fluctuations in the Infrared Caused by Temperature, Humidity and Pressure Fluctuations". J.O.S.A., Vol.70, page 1192, 1980
19	Davidson, K.L. and Houlihan, T.M.	"Turbulence Effects Upon Laser Propagation in the Marine Boundary Layer". Proceedings Society Photo-optical Instrumentation Engineers (Imaging through the atmosphere), Vol.75, page 62, 1976

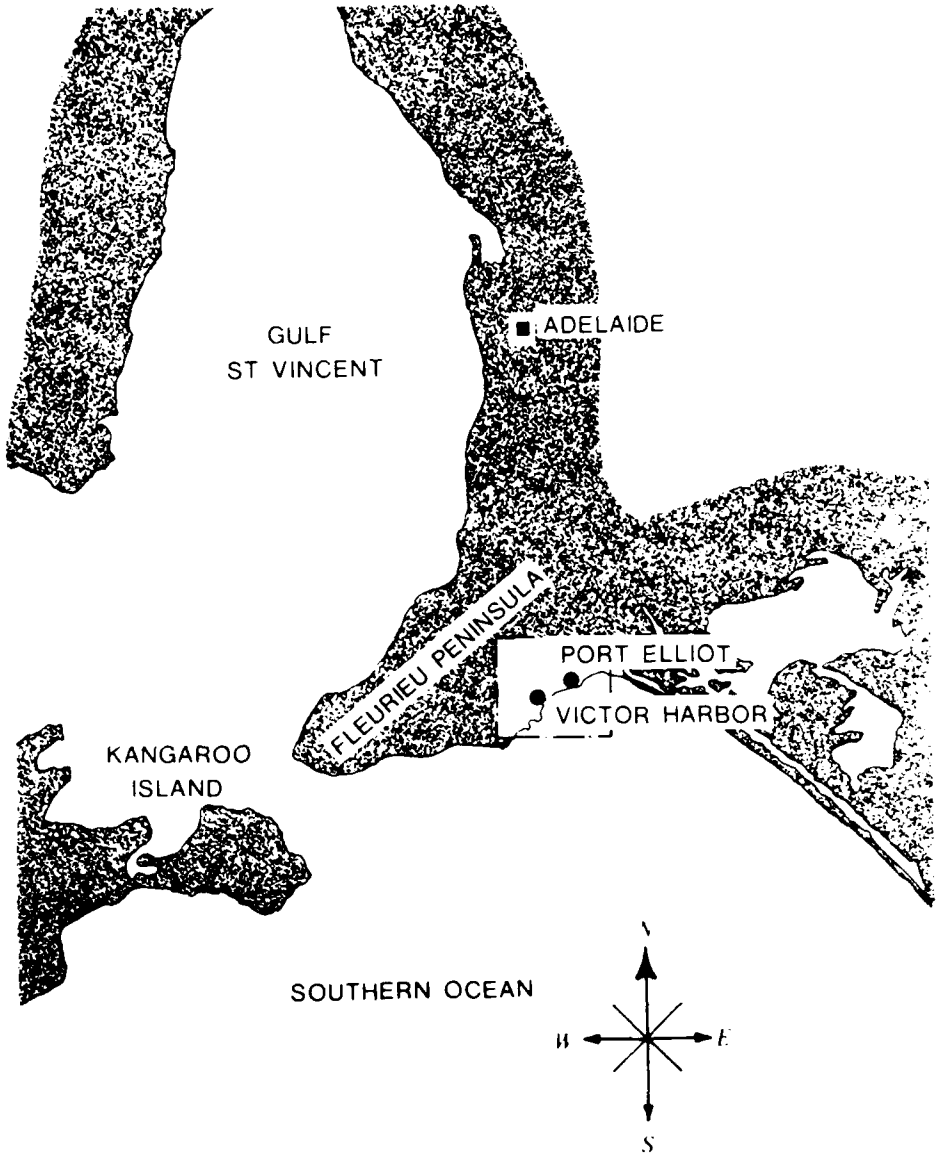

Figure 1. Location of the Victor Harbor transmission measurement site

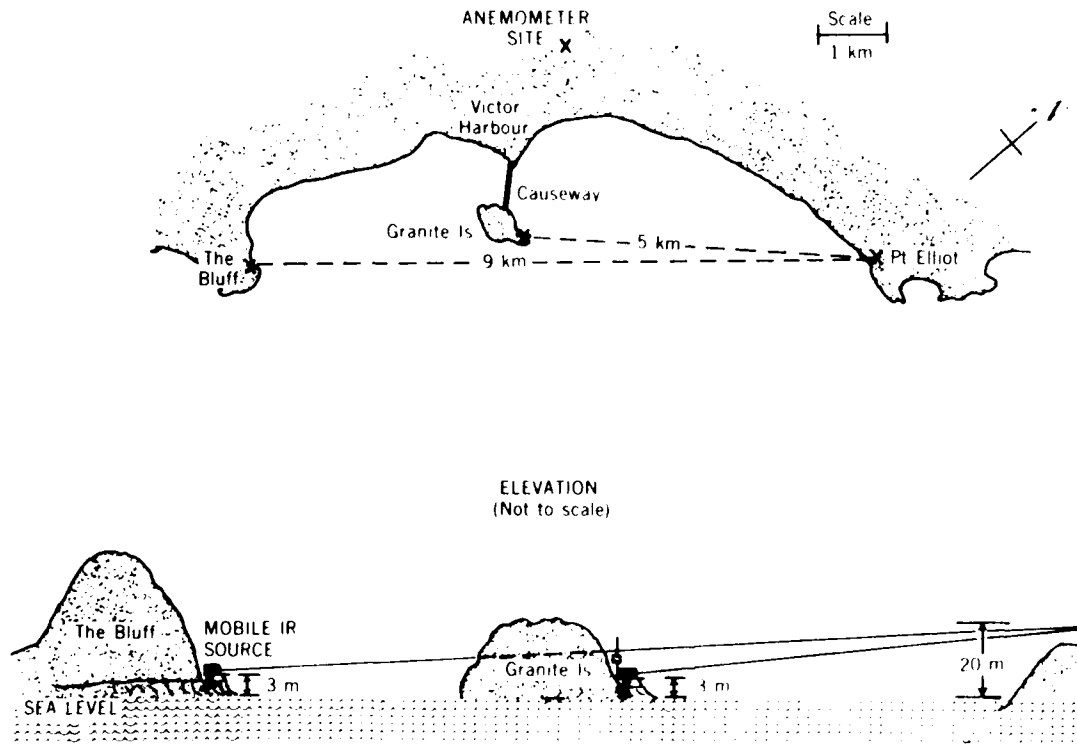

Figure 2. Transmission measurement site layout

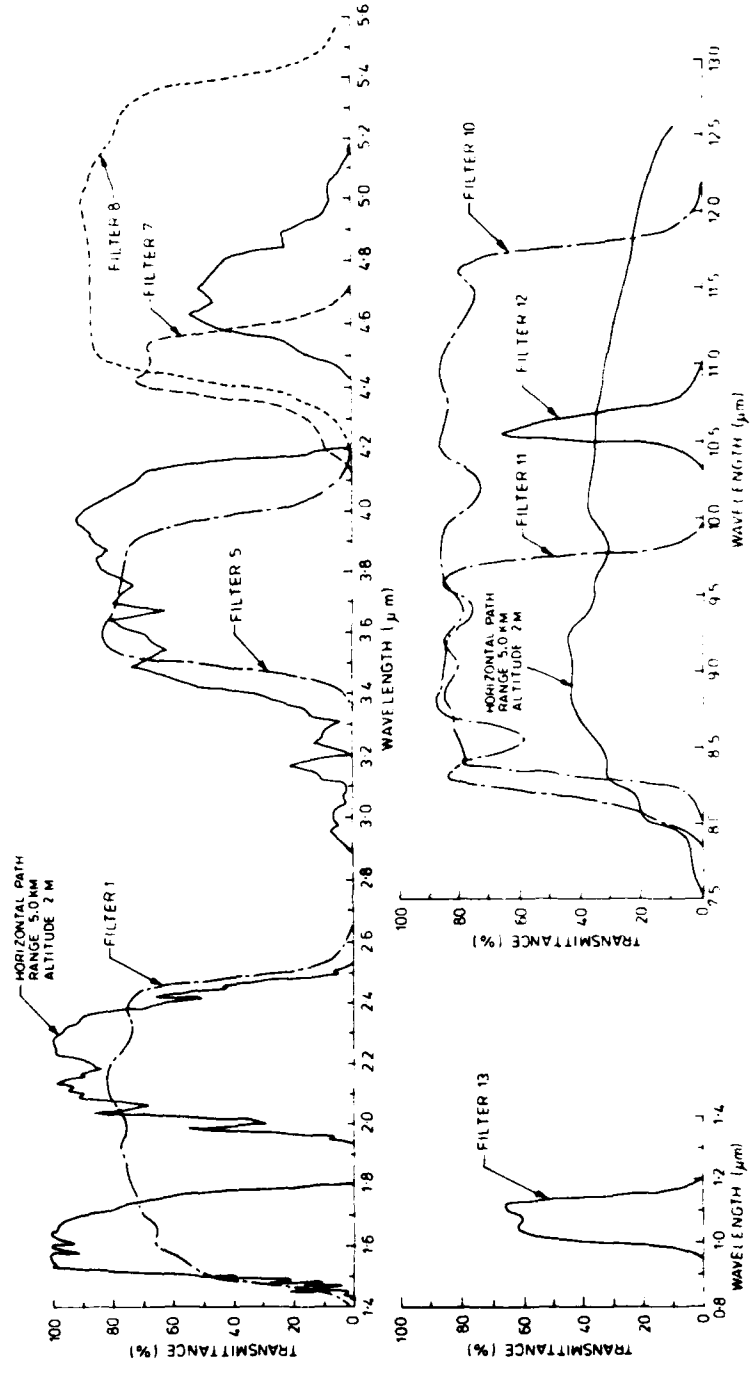

Figure 3. Spectral curves of filters used to define the broadband IR transmission measurement regions.

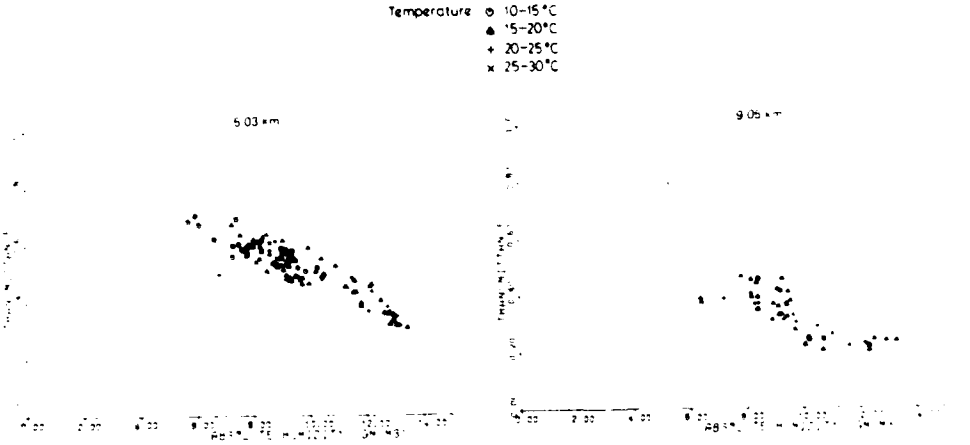

(a) 8.20 μm - 11.76 μm

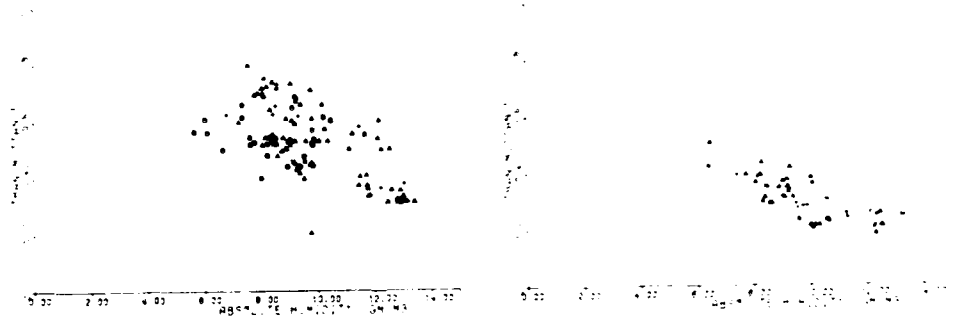

(b) 8.33 μm - 9.80 μm

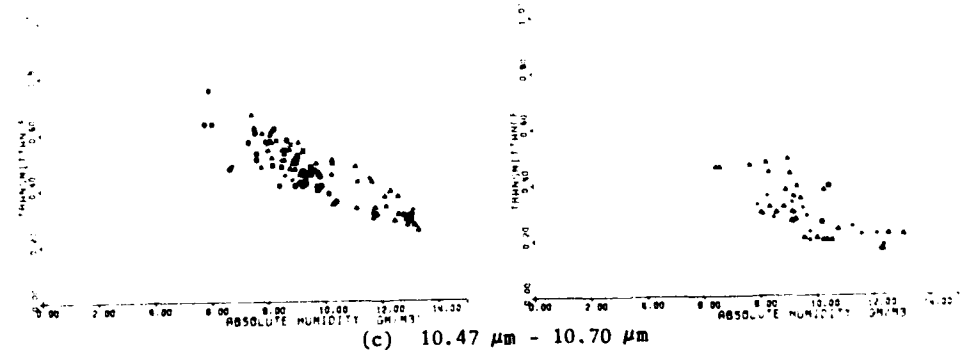

(c) 10.47 μm - 10.70 μm

Figure 4. Atmospheric transmittance versus absolute humidity in the 8.0 to 12.0 μm

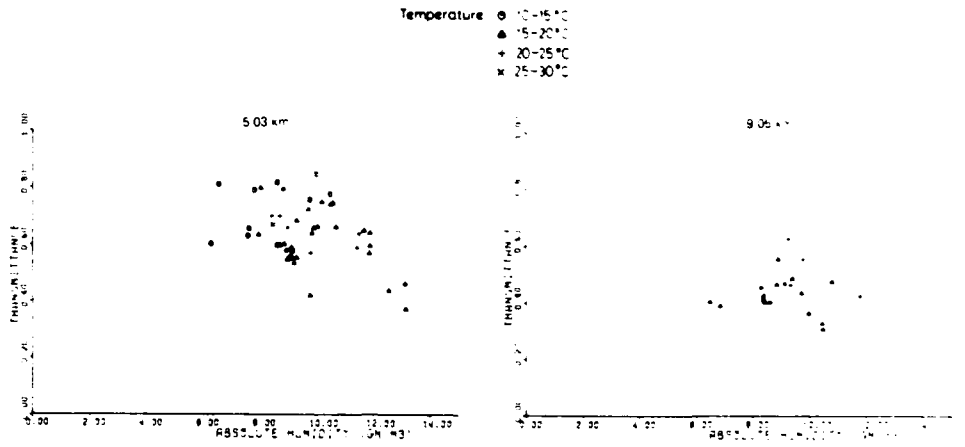

(a) 3.55 μm - 4.00 μm

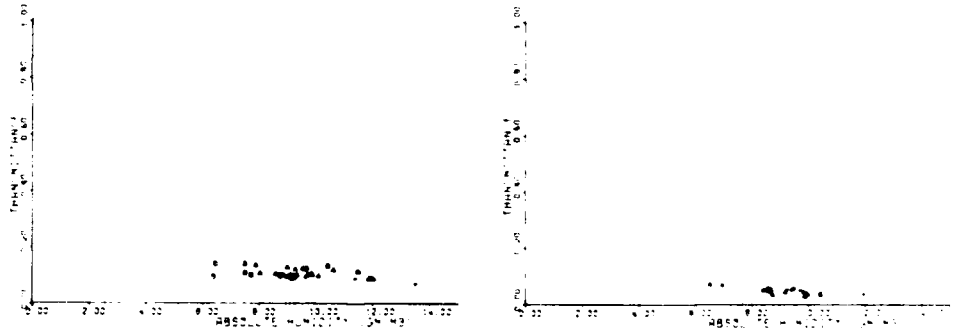

(b) 4.36 μm - 4.59 μm

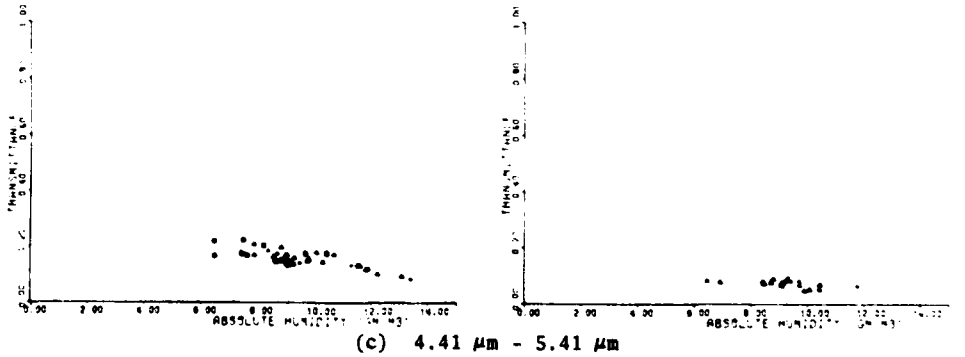

(c) 4.41 μm - 5.41 μm

Figure 5. Atmospheric transmittance versus absolute humidity in the 3.5 to 5.5 μm

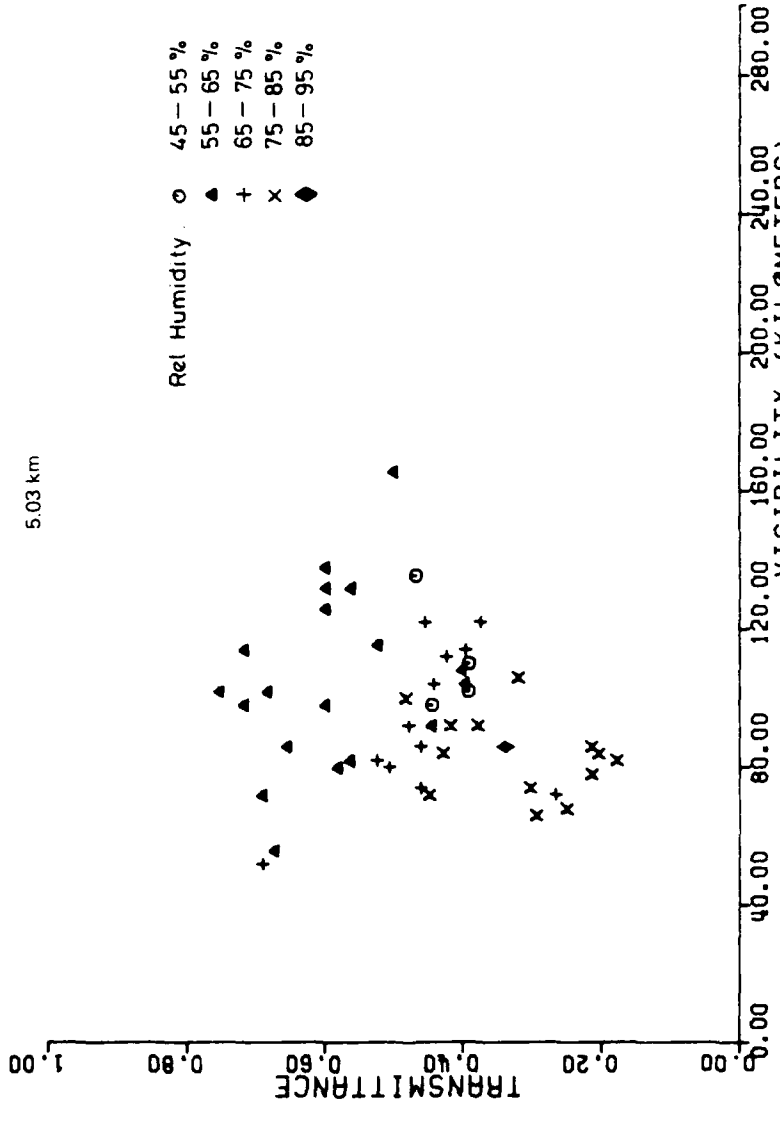

Figure 6. Variation of atmospheric transmittance with visibility for on-shore winds in the spectral region 1.00 to 1.15 μ

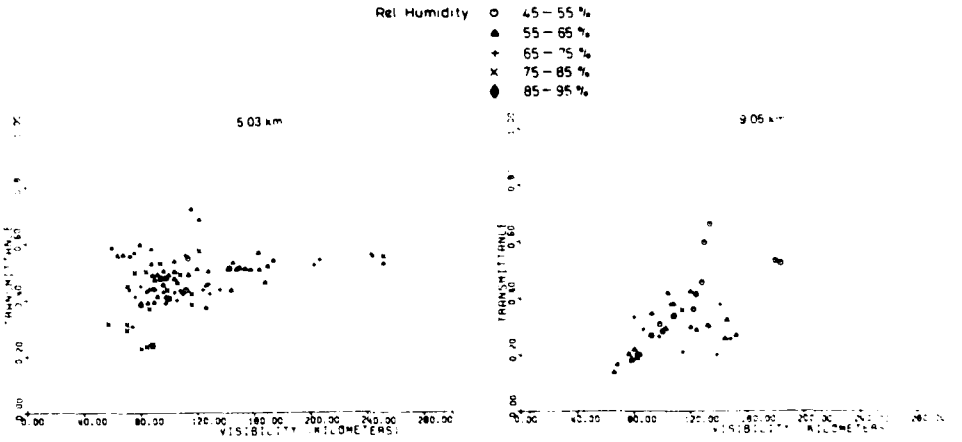

(a) 1.48 μm - 2.50 μm

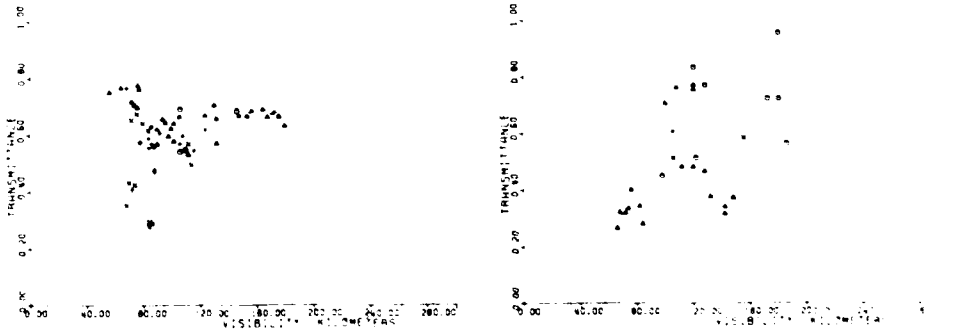

(b) 1.44 μm - 1.82 μm

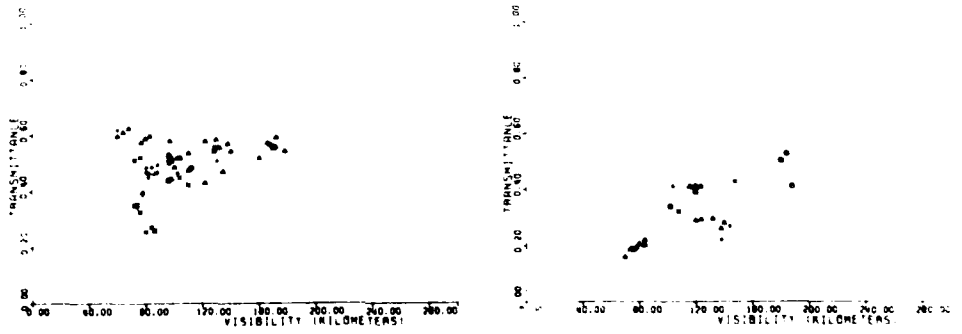

(c) 1.91 μm - 2.47 μm

Figure 7. Atmospheric transmittance versus visibility for on-shore winds in the 1.5 to 2.5 μm spectral region

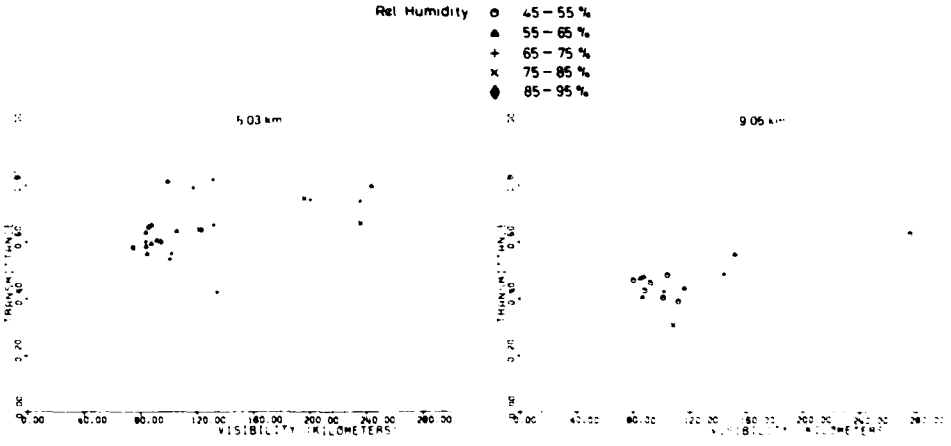

(a) 3.55 μm - 4.00 μm

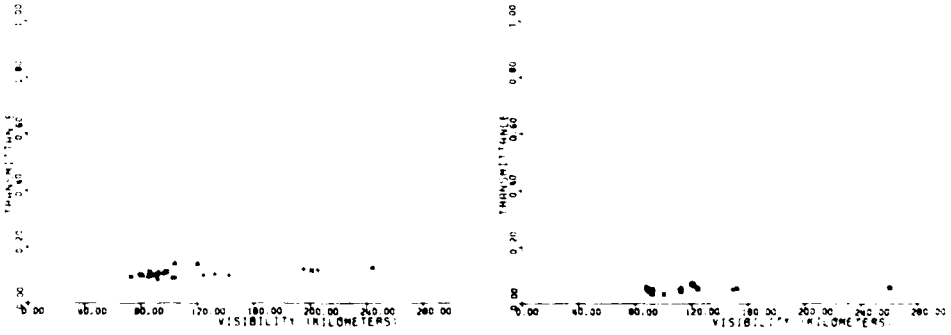

(b) 4.36 μm - 4.59 μm

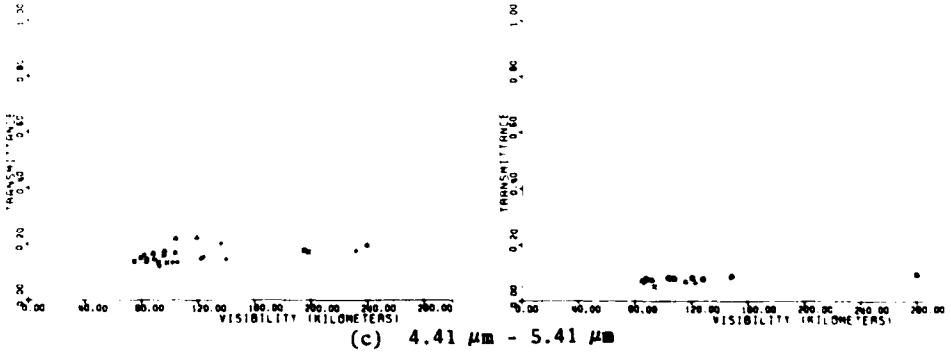

(c) 4.41 μm - 5.41 μm

Figure 8. Atmospheric transmittance versus visibility for on-shore winds in the 3.5 to 5.5 μm spectral region

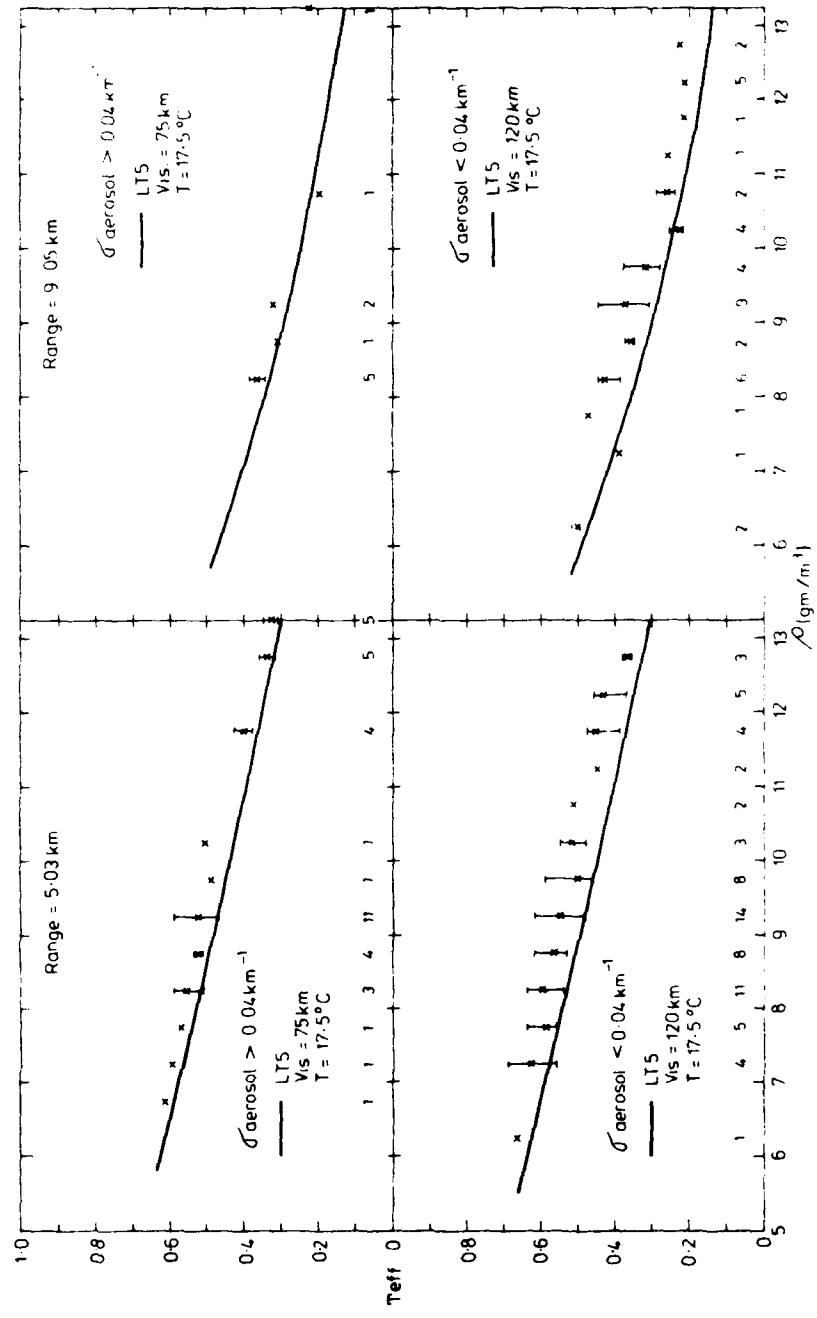

Figure 9. Variation of measured and calculated effective transmittance with absolute humidity in the spectral region 8.20 to 11.8 μm

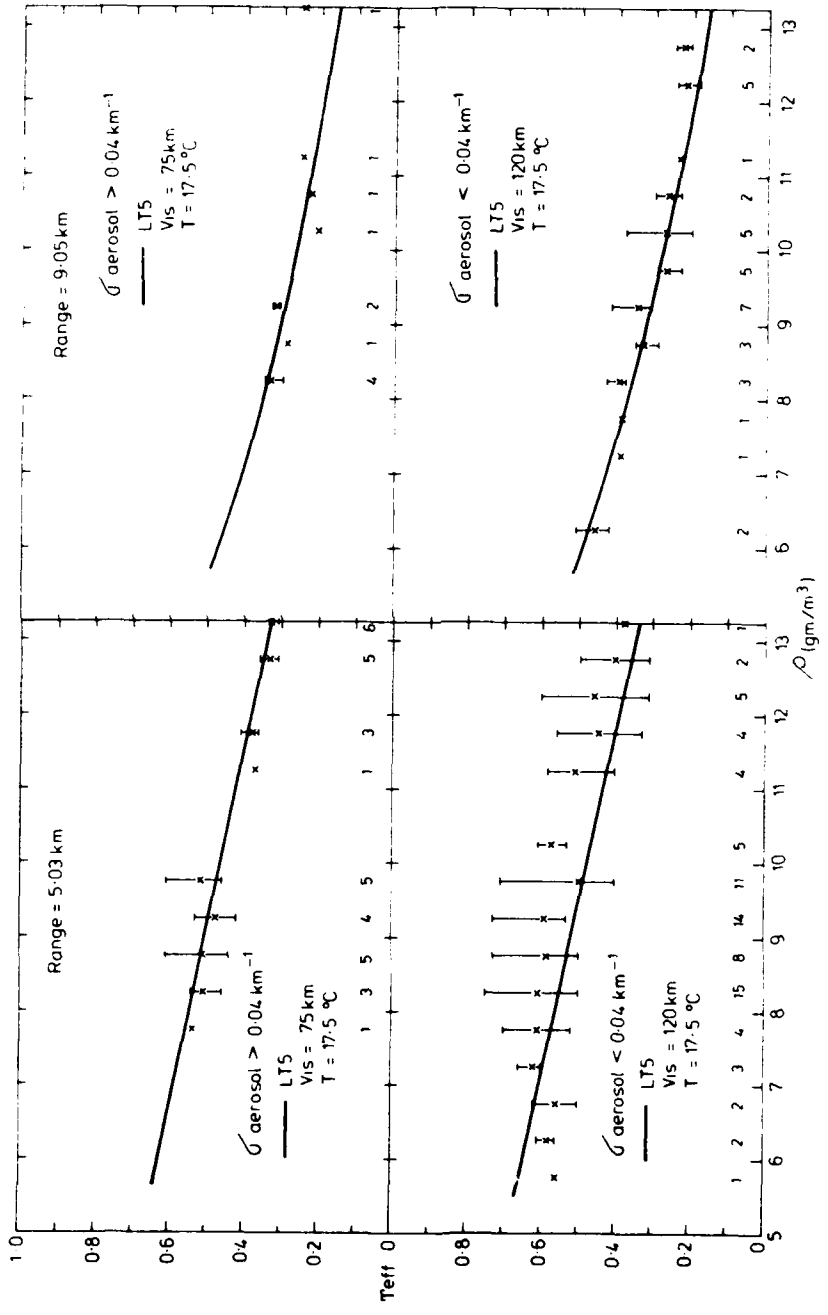

Figure 10. Variation of measured and calculated effective transmittance with absolute humidity in the spectral region 8.33 to 9.80 μm

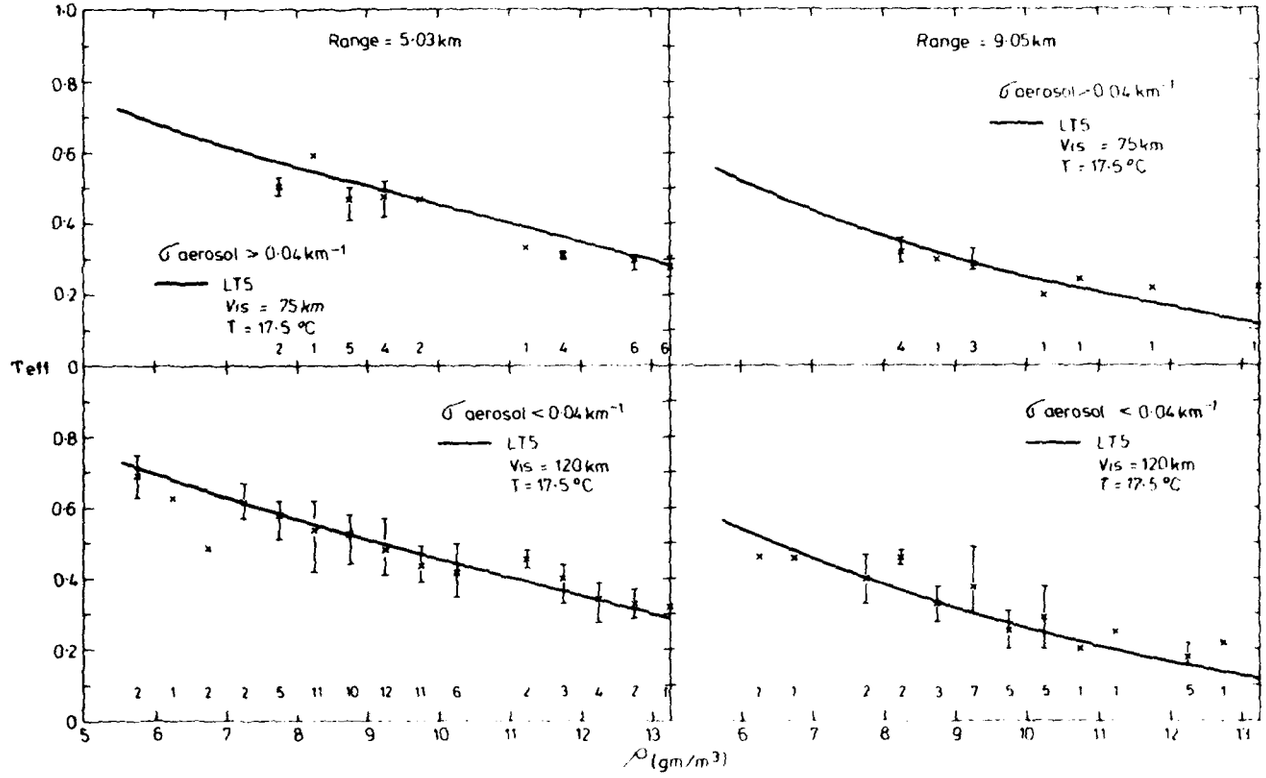

Figure 11. Variation of measured and calculated effective transmittance with absolute humidity in the spectral region 10.5 to 10.7 μm

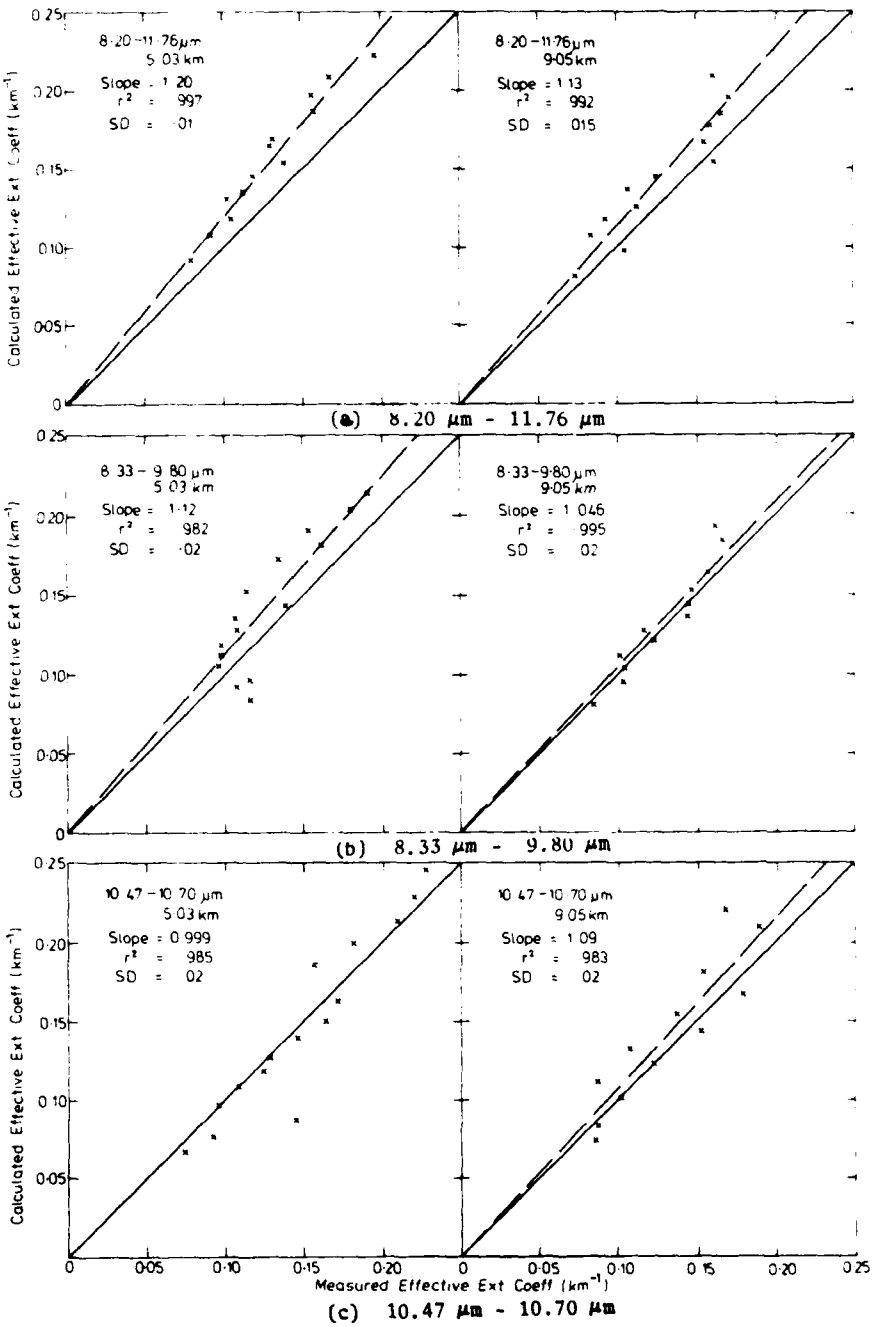

Figure 12. Calculated and measured "effective extinction coefficients" for the 8 to 12 μm spectral region

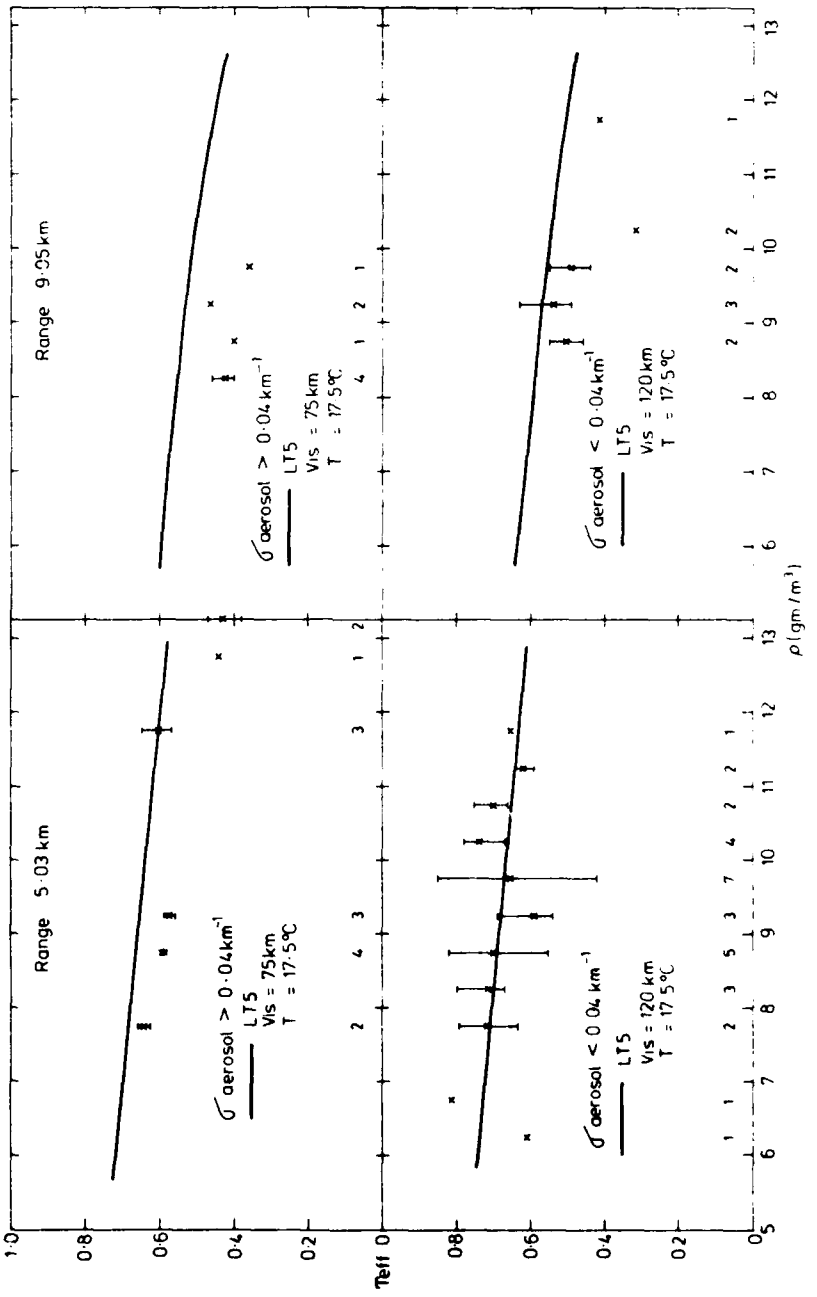

Figure 13. Variation of measured and calculated effective transmittance with absolute humidity in the spectral region 3.55 to 4.00 μm

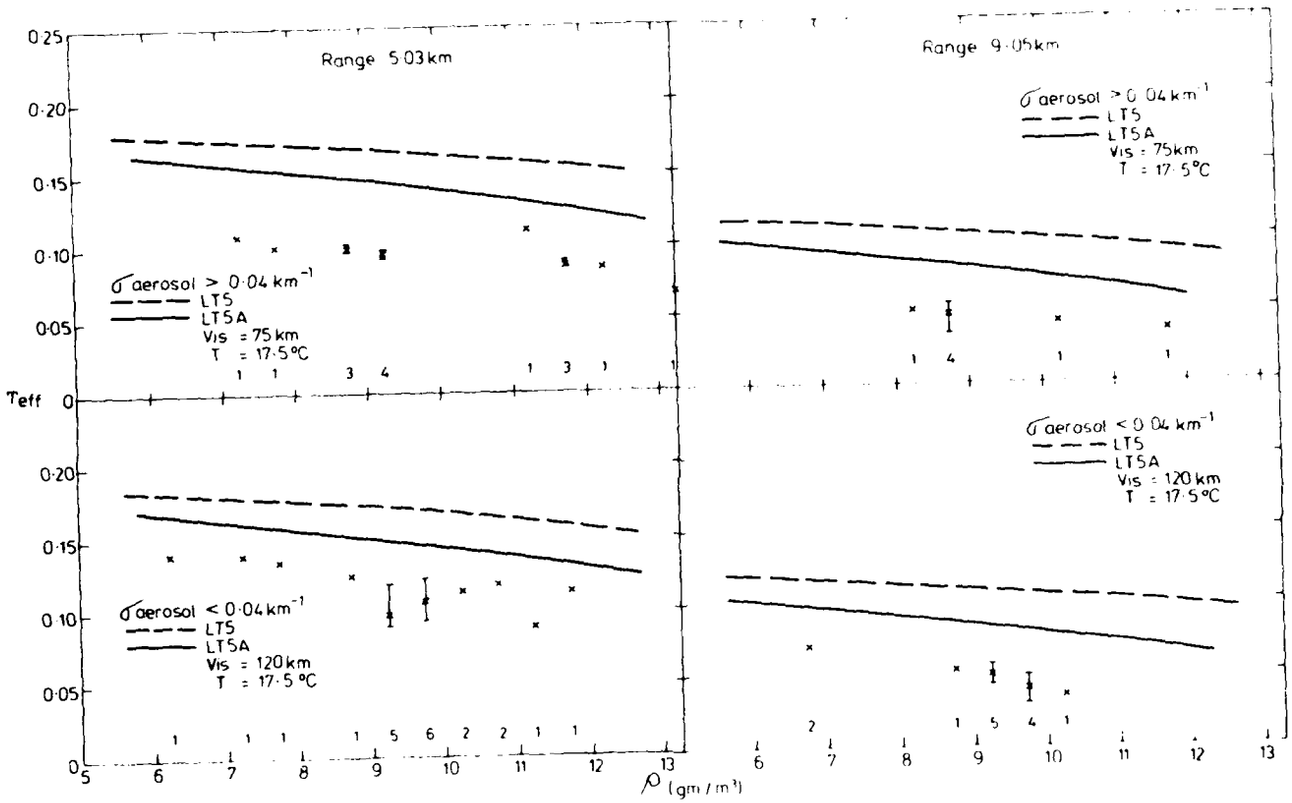

Figure 14. Variation of measured and calculated effective transmittance with absolute humidity in the spectral region 4.36 to 4.59 μm

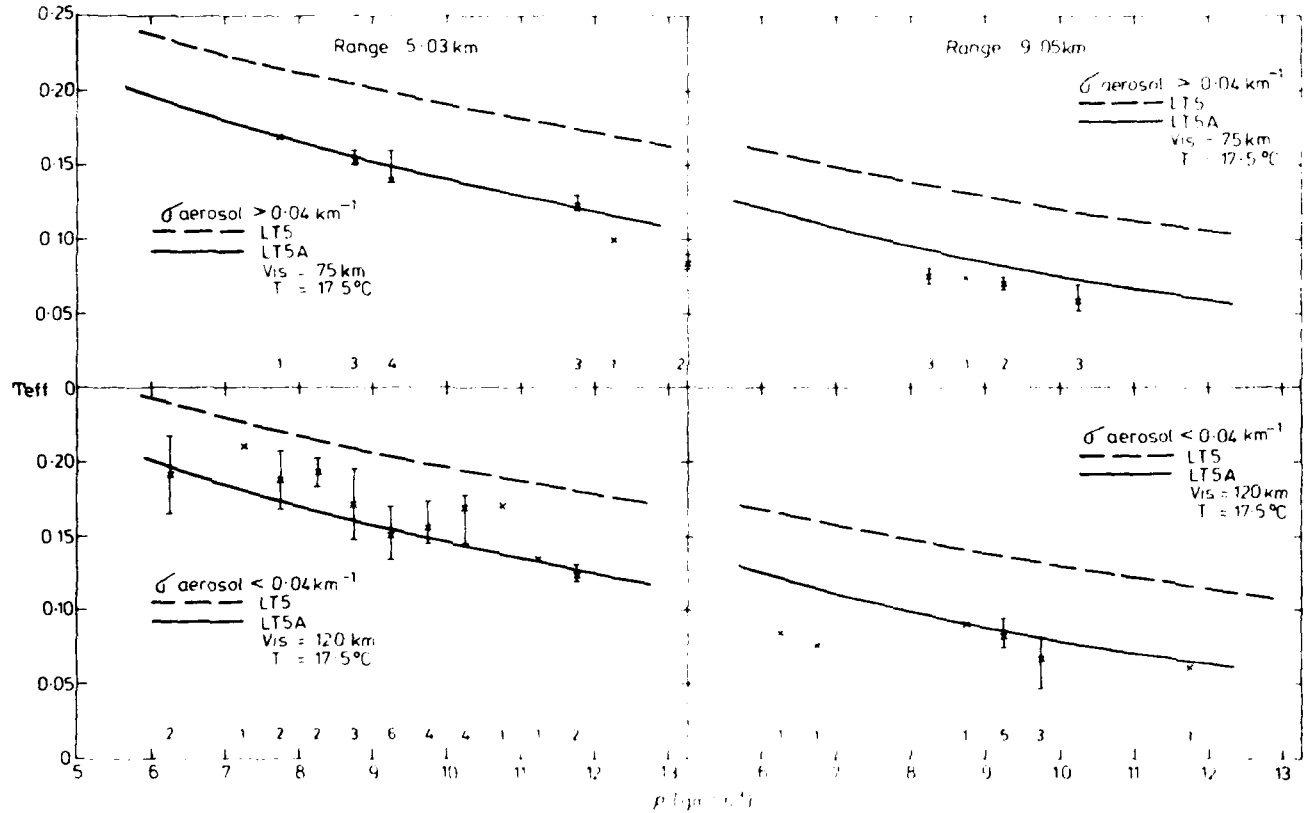

Figure 15. Variation of measured and calculated effective transmittance with absolute humidity in the spectral region 4.11 to 5.11 μm

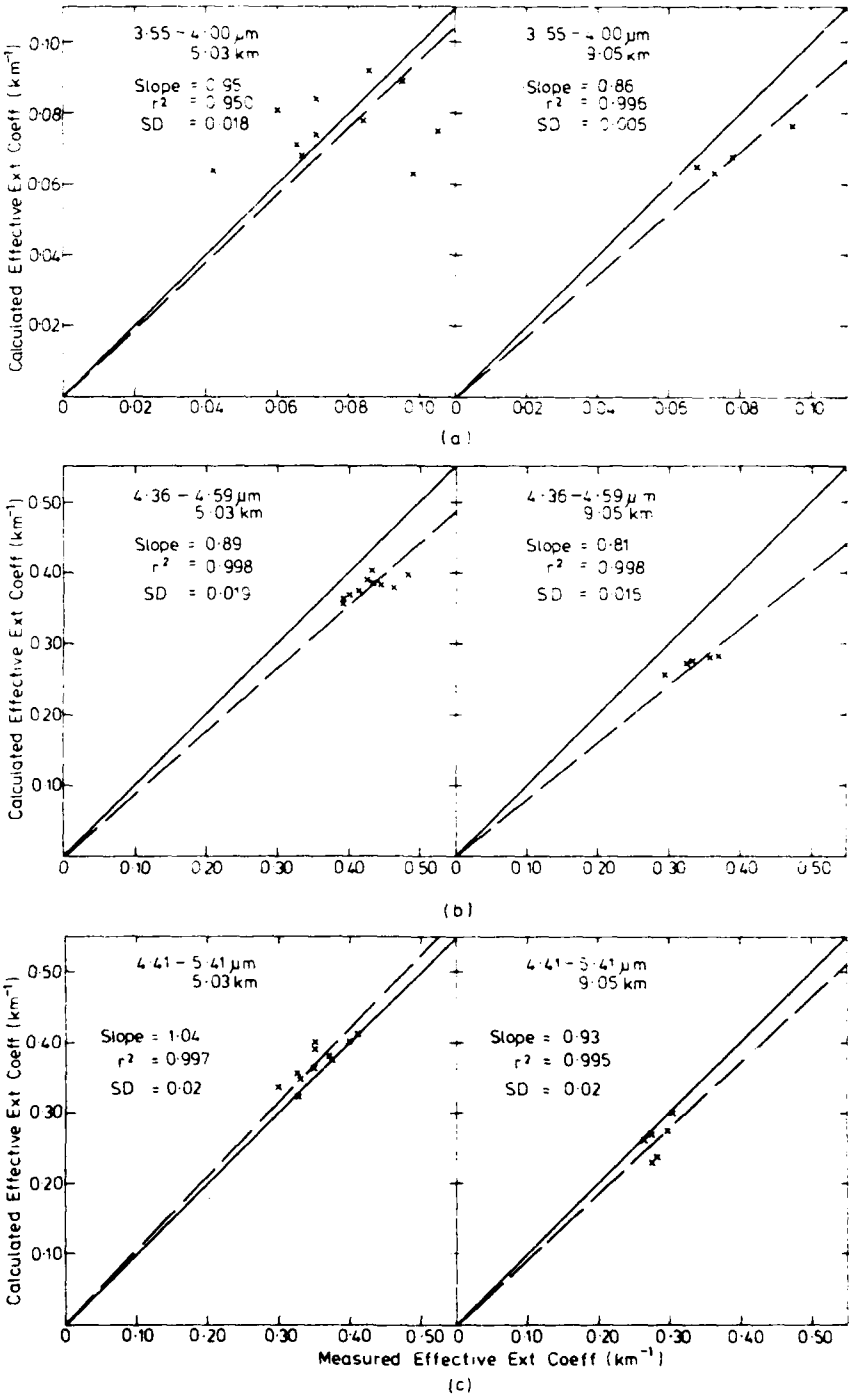

Figure 16. Calculated and measured "effective extinction coefficients" for the 3.5 to 5.5 μm spectral region

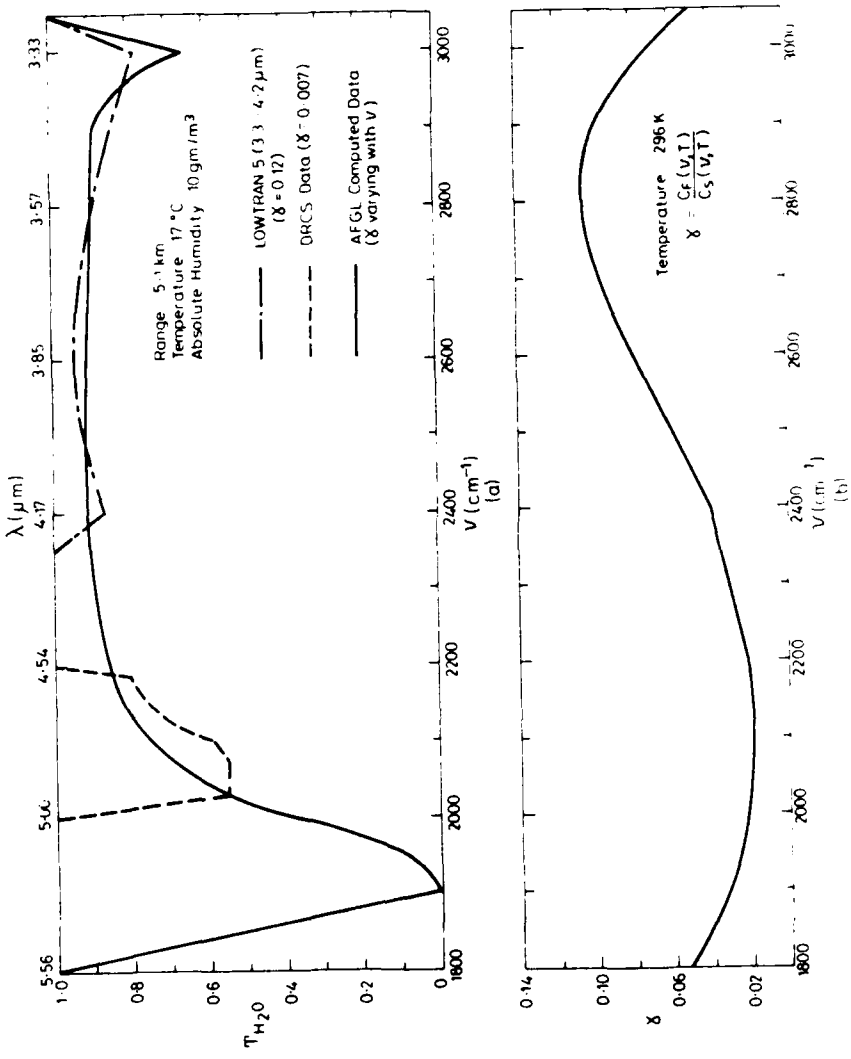

Figure 17. Variation with wavelength of (a) water vapour transmission and (b) γ in the spectral region 3.3 to 5.6 μm

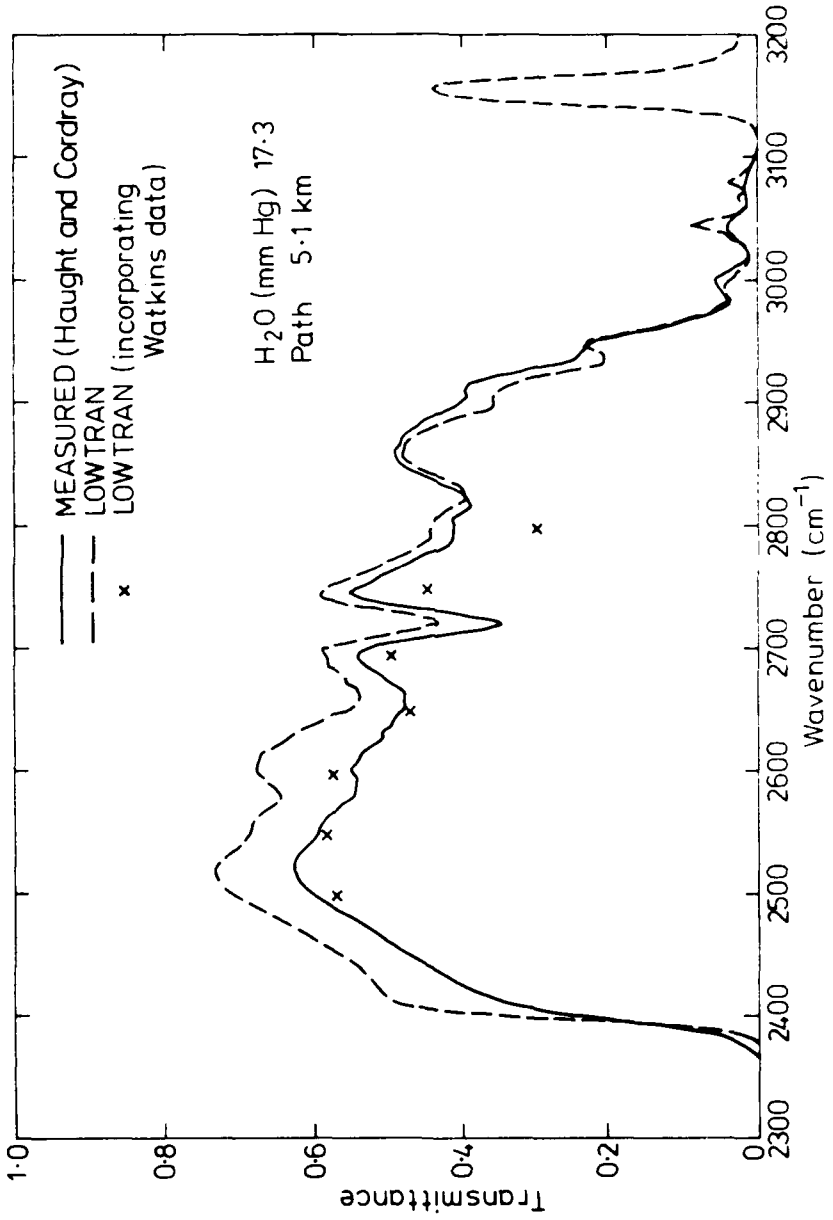

Figure 18. Comparison of Haught and Cordray atmospheric transmittance measurements with LOWTRAN predictions in the 3.5 to 4 μm

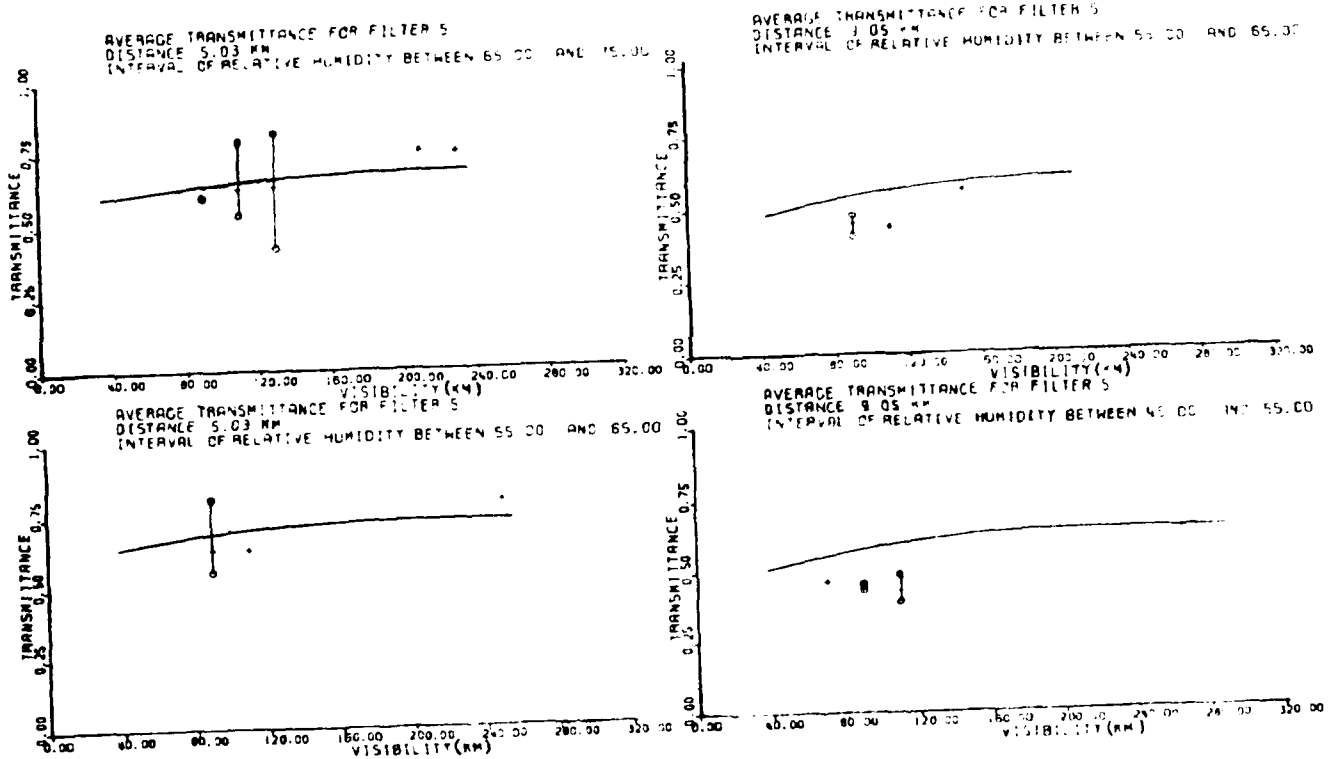

Figure 19. Effective transmittance versus visibility over 5.03 and 9.05 km pathlengths for on-shore winds in the 3.5 to 4.0 μm region

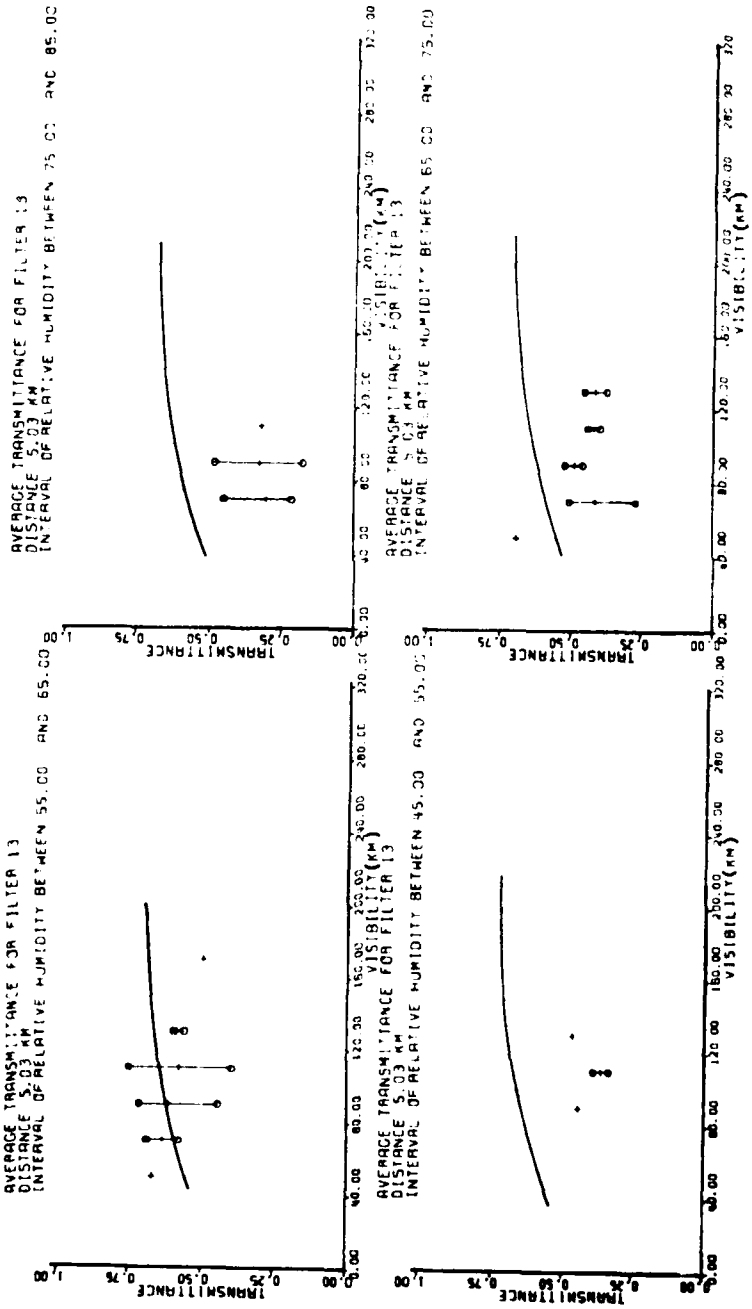

Figure 20. Effective transmittance versus visibility over a 5.03 km pathlength for on-shore winds in the 0.995 to 1.15 μm region

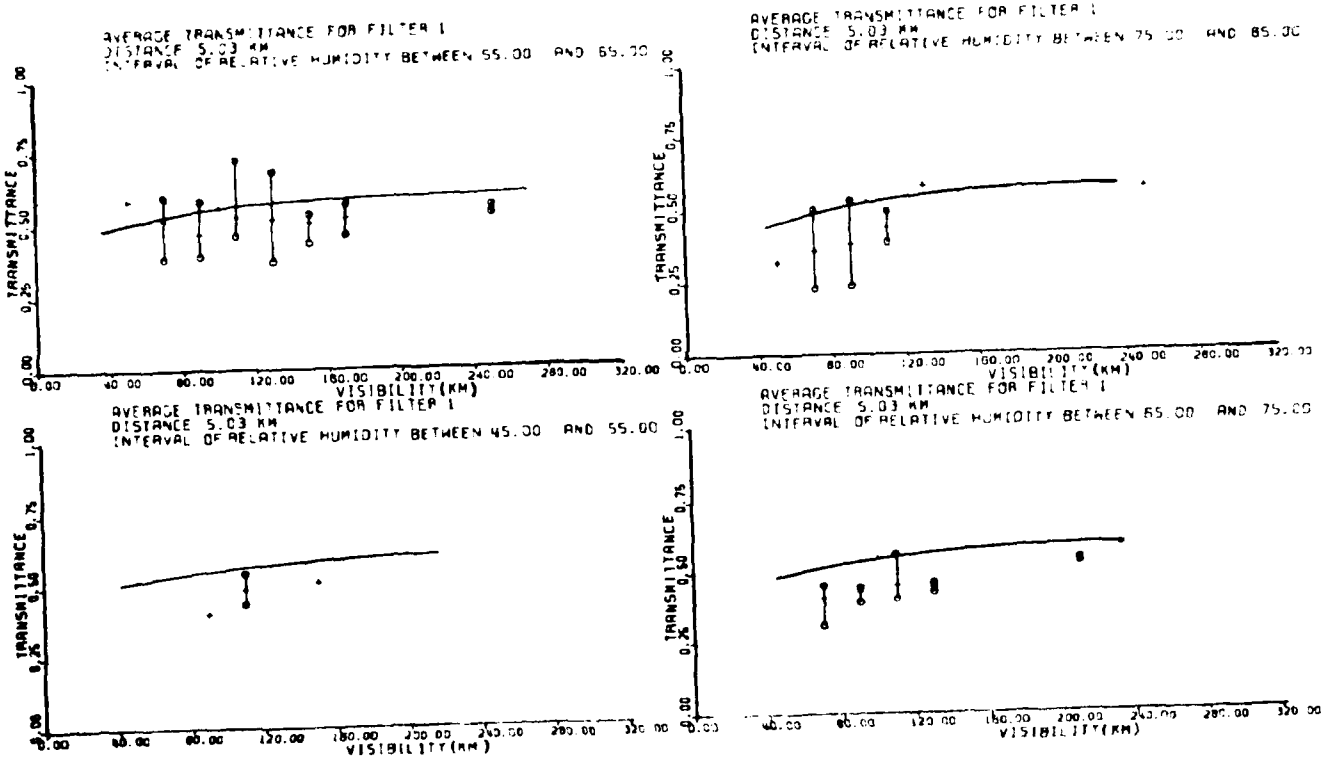

Figure 21. Effective transmittance versus visibility over a 5.03 km pathlength for on-shore winds in the 1.48 to 2.50 μm region

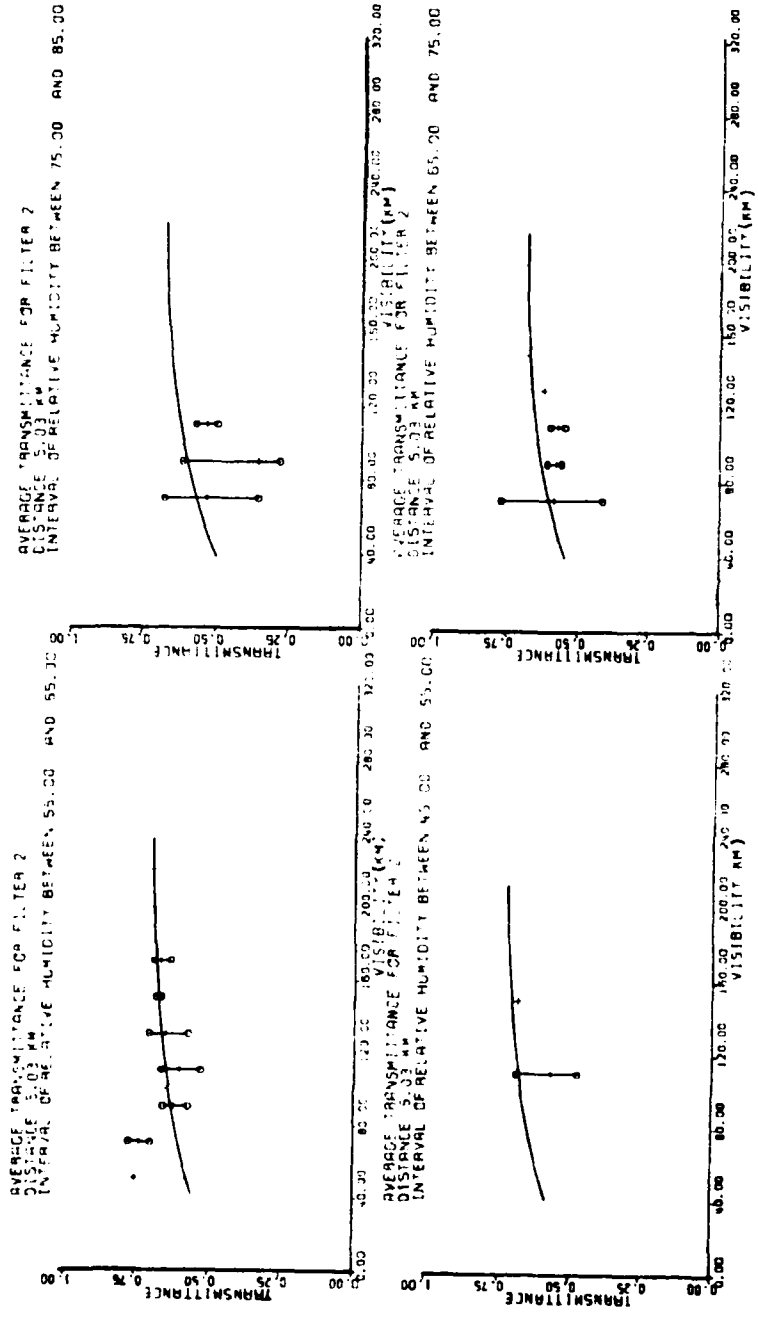

Figure 22. Effective transmittance versus visibility over a 5.03 km pathlength for on-shore winds in the 1.41 to 1.85 μm region

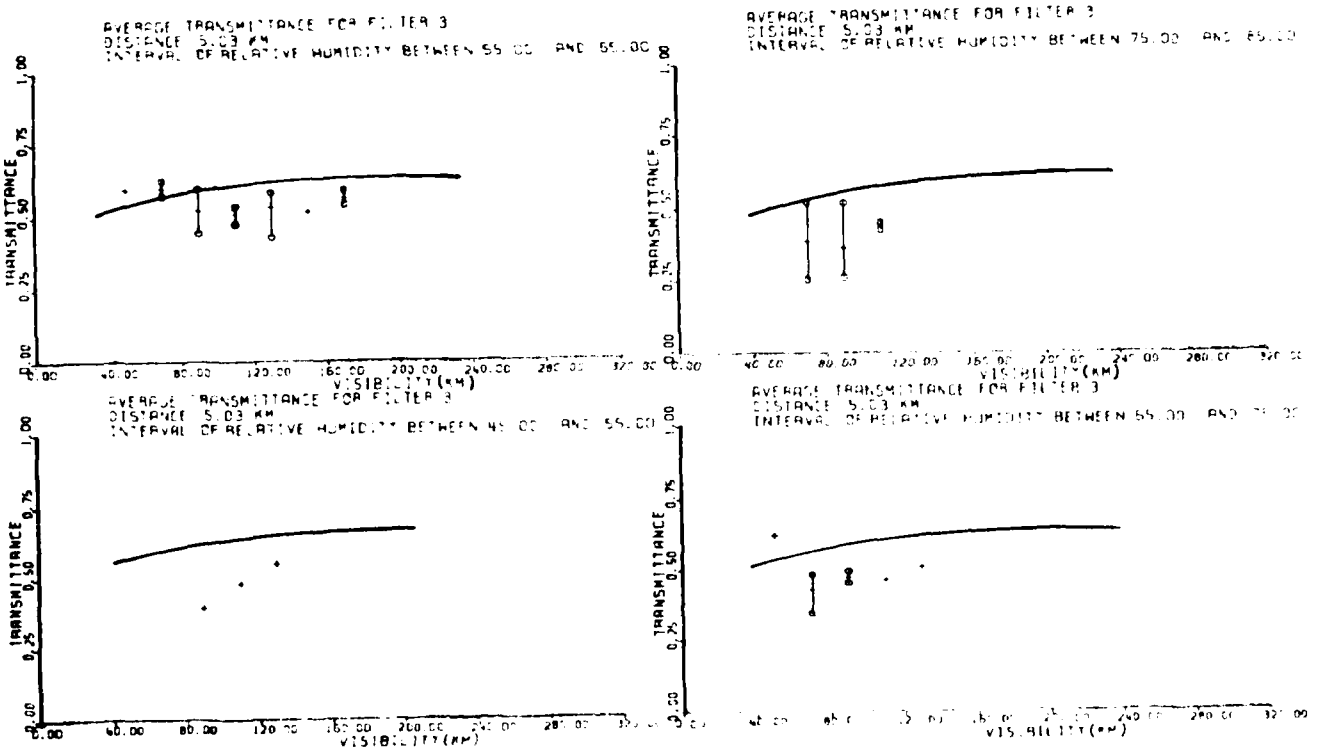

Figure 23. Effective transmittance versus visibility over 5.03 km pathlength for on shore winds, in the 1.91 to 2.41 μ region

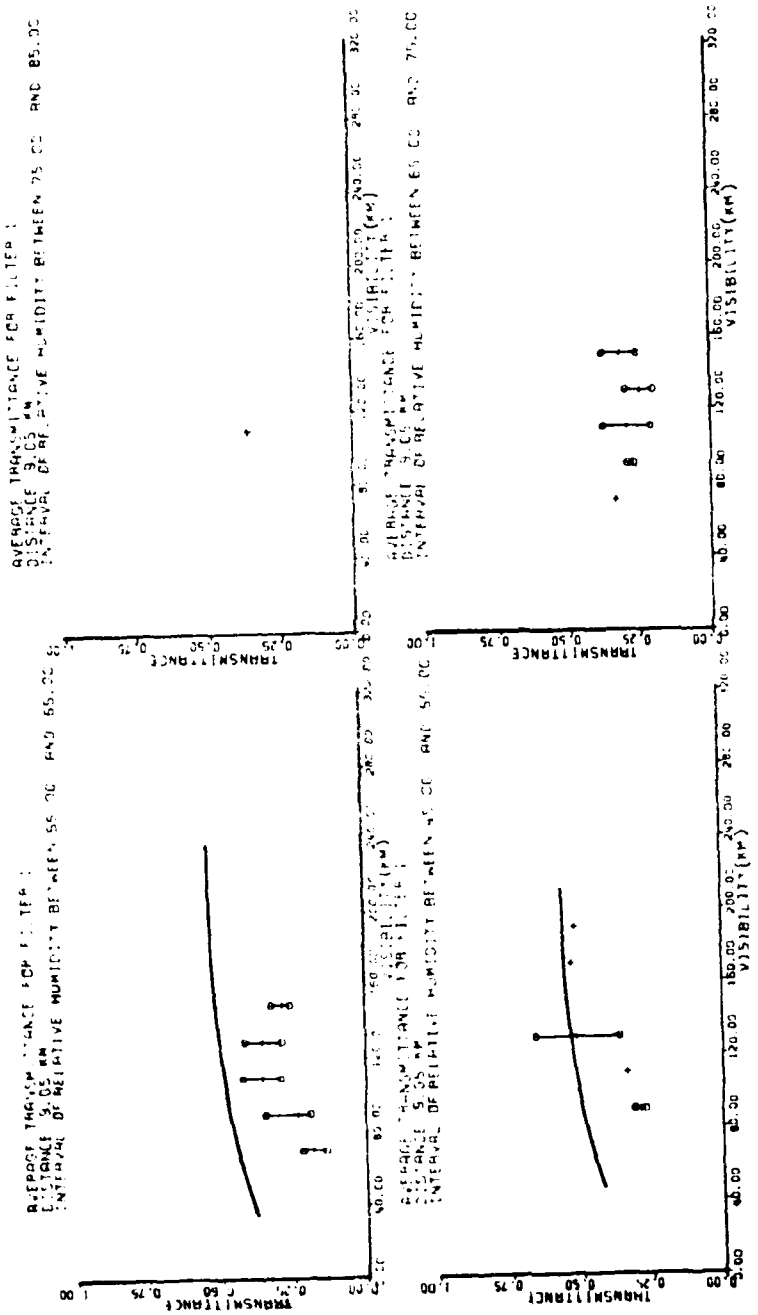

Figure 24. Effective transmittance versus visibility over a 9.05 km pathlength for on shore winds in the 1.4 to 2.5 μm region

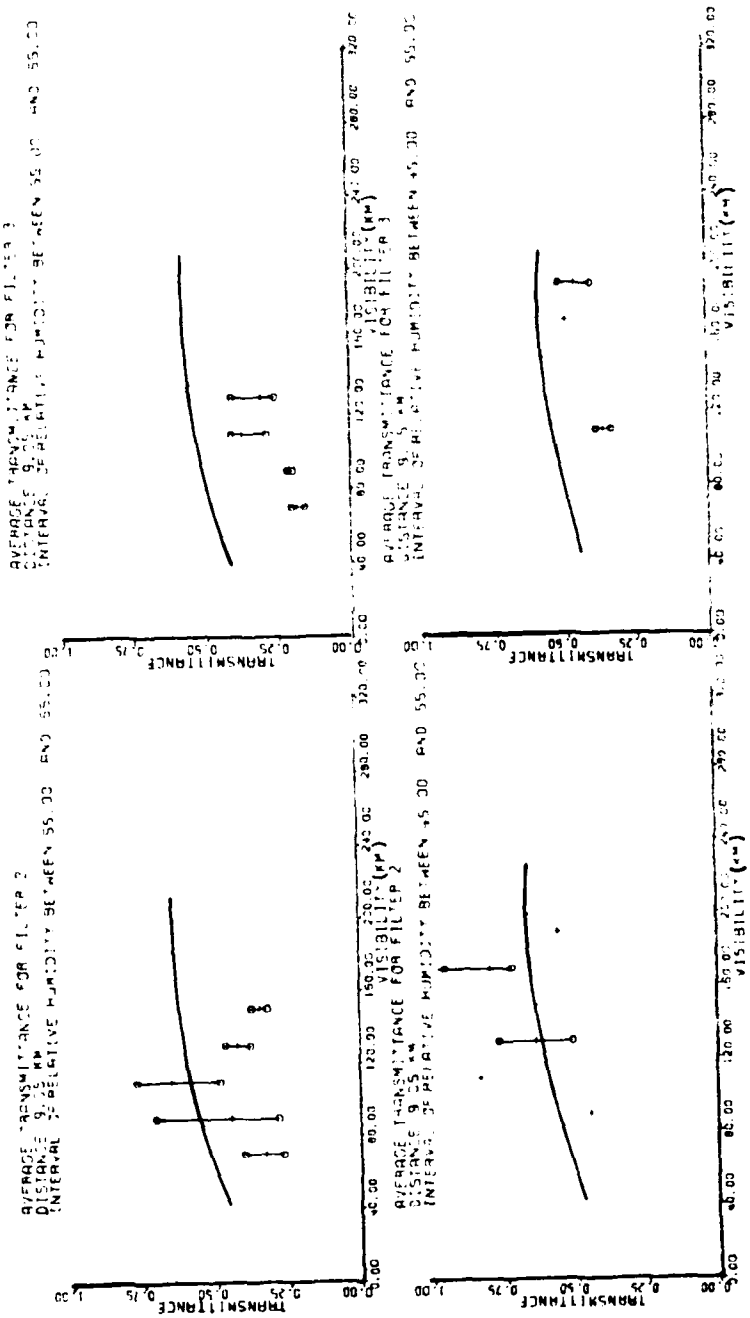

Figure 25. Effective transmittance versus visibility over 9.05 km for on shore winds in the 1.44 to 1.82 μm and 1.91 to 2.47 μm regions

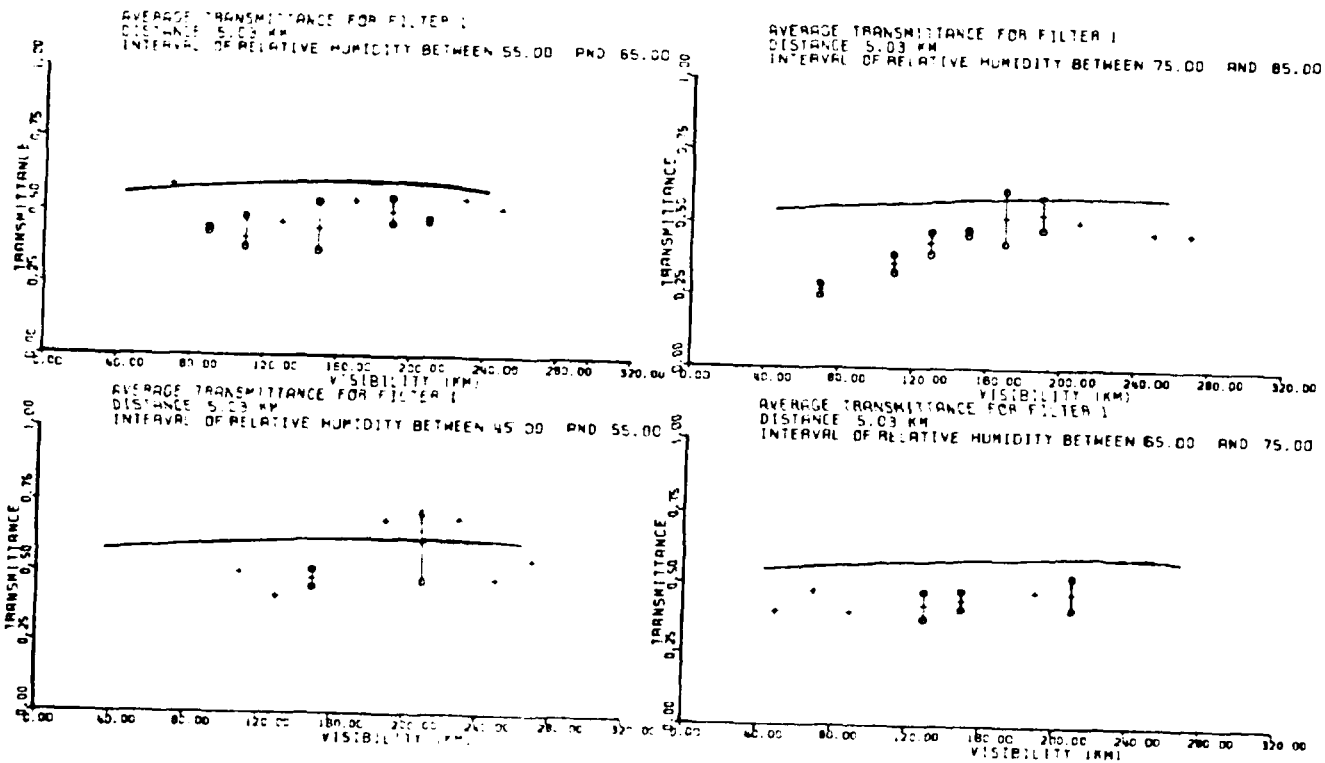

Figure 26. Effective transmittance versus visibility over 5.03 km pathlength for off shore wind in the 1.15 to 2.50 μm region

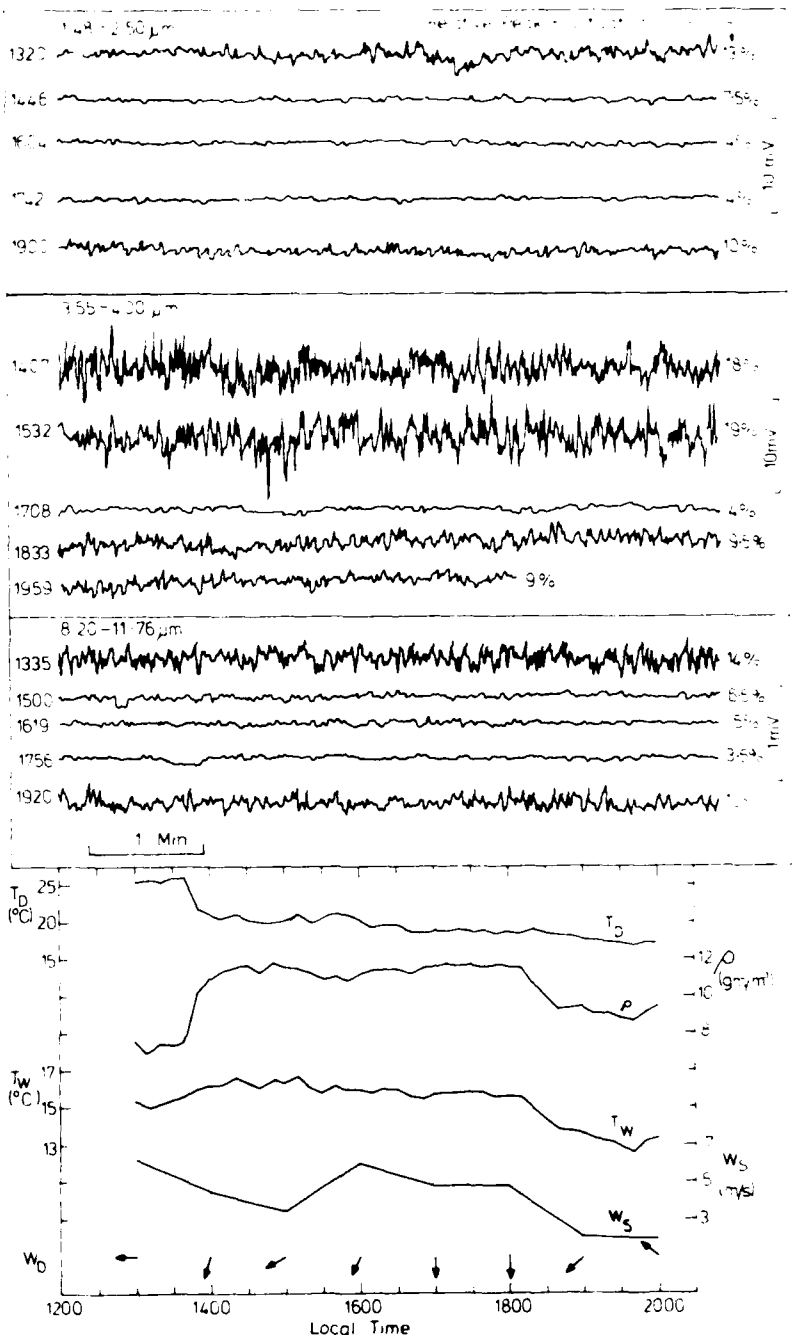

Figure 27. Signal fluctuations recorded over 5.03 km during the passage of a cold front across the measurement site on 31/10/79

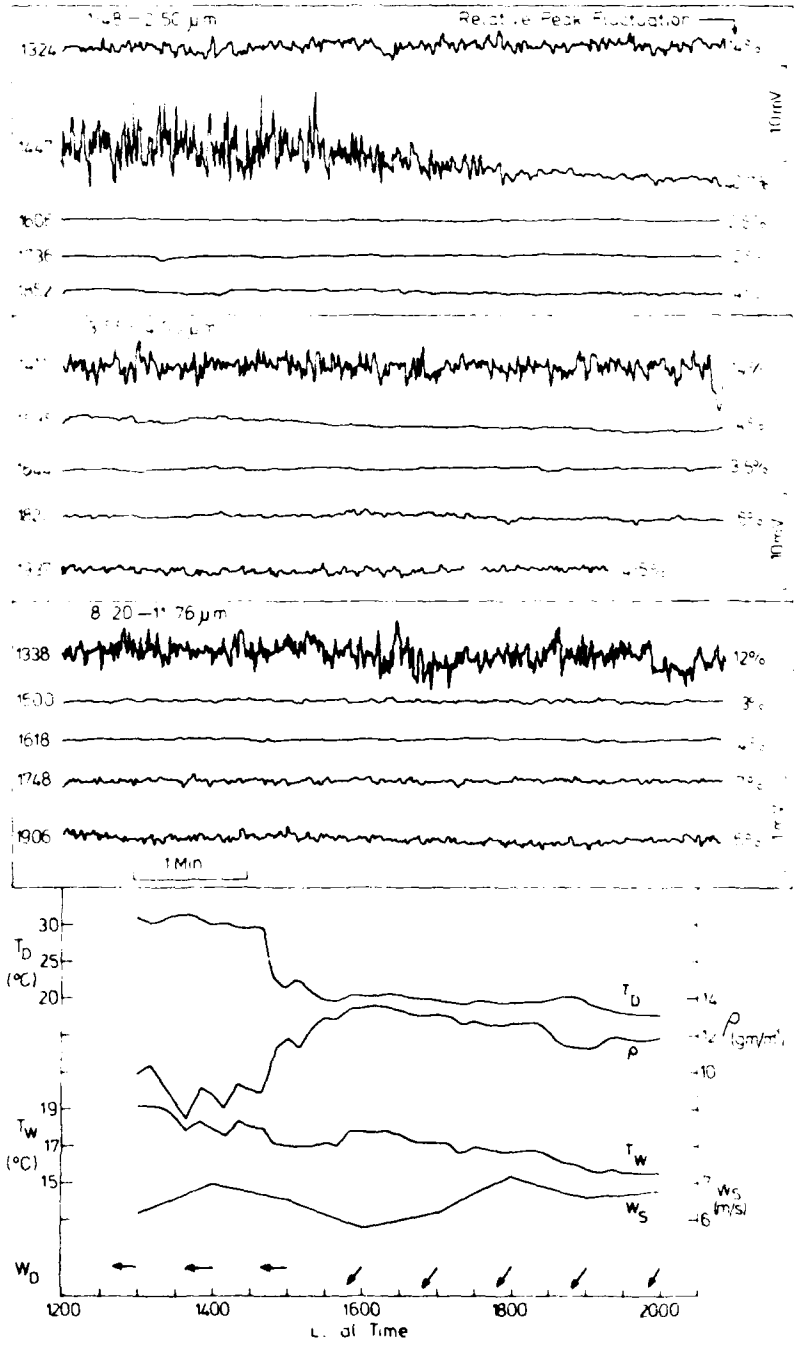

Figure 28. Signal fluctuations recorded over 5.03 km during the passage of a cold front across the measurement site on 4/12/79

APPENDIX I

EFFECTIVE TRANSMITTANCE MEASUREMENT EQUATION

I.1 Derivation of measurement equation

This section briefly describes the derivation of the equation which is used to convert the signal voltages developed by the filter/detector combinations in the radiometer into values of effective transmittance (T_{eff}).

The irradiance, $H_{\Delta\lambda}$(w cm^{-2}), at the radiometer over the spectral bandwidth, $\Delta\lambda$, due to the point source at range, R, is

$$H_{\Delta\lambda} = J_{\Delta\lambda}\, T_{eff}(\Delta\lambda,R)/R^2 \qquad (I.1)$$

where $J_{\Delta\lambda}$ is the source radiant intensity (w sr^{-1}) for the wavelength interval, $\Delta\lambda$, and $T_{eff}(\Delta\lambda,R)$ is the effective atmospheric transmittance over the filter bandwidth, $\Delta\lambda$.

Integrating over the spectral bandpass of the filter, $\Delta\lambda$, and substituting for $J_{\Delta\lambda}$, gives the total received signal as follows

$$V = \frac{\epsilon^1 A_s A_R K R^1_{\Delta\lambda} T_{eff}(\Delta\lambda, R)}{\pi R^2} \int_{\Delta\lambda} w^1(\lambda, T)\, T_F(\lambda)\partial\lambda \qquad (I.2)$$

where $w^1(\lambda,T)$ = radiant emittance (w cm^{-2}) from the field black-body source at absolute temperature T,

ϵ^1 = emissivity of the field black-body sorce,

$T_F(\lambda)$ = spectral response of the band-pass filter,

A_s = area of source aperture,

A_R = area of receiving optics aperture,

K = obscuration due to "venetian-blind" type chopper blades, and

$R^1_{\Delta\lambda}$ = radiometer responsivity (V w^{-1}) averaged over the filter bandwidth, $\Delta\lambda$.

$w^1(\lambda,T)$ for the field source is determined in the laboratory from surface temperature measurements (see reference 3). The radiometer responsivity $R^1_{\Delta\lambda}$ is determined in the laboratory(ref.3) using a standard black-body source located at the focus of a collimating mirror (focal length 5 m) and set to a temperature near the average temperature of the field source. Generally 3 apertures were used to determine the least squares linear fit to the V_i versus A_i data. Thus using equation (I.2) it follows that:

$$R'_{\Delta\lambda} = \epsilon \cdot \frac{1}{\int_{\Delta\lambda} w(\lambda,T)\ T(13,\lambda)\ T_F(\lambda)\partial\lambda} \cdot \frac{\pi F^2}{R_M A_R K} \cdot \sum_{i=1}^{3} \frac{V_i A_i}{A_i^2} \qquad (I.3)$$

where $T(13,\lambda)$ = atmospheric transmittance for a 13 m calibration pathlength,

V_i = radiometer voltage output for source aperture A_i,

R_M = reflectance of the collimating mirror.

F = focal length of the collimating mirror.

Note that K also appears in equation (I.3) because the same chopper is used. Combining equations (I.2) and (I.3) results in

$$T_{eff}(\Delta\lambda,R) = \frac{\epsilon W_{\Delta\lambda}}{F^2} \cdot \frac{R_M}{\epsilon' W'_{\Delta\lambda}} \cdot \frac{VR^2}{GA_S} \cdot \frac{1}{R_{\Delta\lambda}} \qquad (I.4)$$

where

$$W_{\Delta\lambda} = \int_{\Delta\lambda} \omega(\lambda,T)T(13,\lambda)T_F(\lambda)d\lambda,$$

$$W'_{\Delta\lambda} = \int_{\Delta\lambda} \omega'(\lambda,T)T_F(\lambda)d\lambda,$$

and

$$R_{\Delta\lambda} = \sum_{i=1}^{3} \frac{V_i A_i}{A_i^2}$$

The gain factor G for the amplifiers has been included in equation (I.4). In measuring $R_{\Delta\lambda}$ the choice of temperature for the standard black-body source is not critical since for small temperature changes (eg ±10K) around 980 K, the radiant flux changes with black-body temperature are almost linear for the spectral region 1 to 12 μm and the error arising can be neglected.

I.2 Expression for calculating effective transmittance from spectral transmittance

The atmospheric transmittance data are obtained with a transmissometer that includes a source, filter and detector that have spectral characteristics over the wavelength interval $\Delta\lambda$. Hence, the measured transmittance $T_{eff}(\Delta\lambda,R)$ is not the average of the spectral transmittance $T(\lambda,R)$ for the

interval $\Delta\lambda$ but is, in fact, the average value of the combination of $T(\lambda,R)$, the source, filter and radiometer spectral curves. To compare the measured values of transmittance with the theoretical spectral transmittance values derived from, say LOWTRAN 5 computations, the source, filter and radiometer spectral curves must be determined and included in the calculations. The equation which combines all these curves with $T(\lambda,R)$ takes the form

$$T_{eff} = \frac{\int_{\Delta\lambda} w(\lambda,T)\ T_F(\lambda)\ T(\lambda,R)\ R(\lambda)\partial\lambda}{\int_{\Delta\lambda} w(\lambda,T)\ T_F(\lambda)\ R(\lambda)\partial\lambda} \qquad (I.5)$$

where $R(\lambda)$ is the spectral responsivity ($Vw^{-1}\ \mu m^{-1}$) of the radiometer detector. If $w(\lambda,T)$, $T_F(\lambda)$ and $R(\lambda)$ are constant over the spectral band $\Delta\lambda$ (which would generally be the case if $\Delta\lambda$ is small) then:

$$T_{eff} = \frac{1}{\Delta\lambda}\int_{\Delta\lambda} T(\lambda,R)\partial\lambda = T_{ave} \qquad (I.6)$$

Except for filter 7, the values of T_{eff} and T_{ave} differ by no more than 0.025 transmittance for values between 0.2 and 0.75. For effective transmittance calculations made in this report using LOWTRAN 5 data, the source spectral response was assumed to be a black-body spectral radiance curve at T=990 K, the spectral curves of the individual band-pass filters were measured with a spectrometer, and the detector response curves supplied by the manufacturers used for $R(\lambda)$. The gold coatings on the mirrors in the radiometer and the "Glad-Wrap" window were assumed to have a constant spectral response over the wavelength region $\Delta\lambda$.

APPENDIX II

ERROR ANALYSIS FOR THE MEASUREMENT OF ATMOSPHERIC TRANSMITTANCE

II.1 Introduction

There is always difficulty in determining the precise magnitude of the errors both relative and absolute associated with the measurement of atmospheric transmittance using transmissometers. The only thing that can really be done is to identify the individual sources of error (both operational and instrumental), estimate their magnitudes and then combine them according to existing laws on errors which will give lower and upper boundaries. The estimation of component error magnitudes has to be based on laboratory measurements, field measurements and operator experience with the instrumentation.

II.2 Error estimates

There are generally two methods of estimating errors associated with measuring transmittance. They are:

(i) An external estimate of the relative and absolute errors E_e which are obtained from a knowledge of the instrumentation and experiment.

(ii) An internal estimate of the error E_i based on analysis of the experimental data itself, eg by determining the mean value and standard deviation of a group of data from several transmissometers operating at the same time side by side.

In this section, error analysis will be devoted to errors of the external type as no comparisons of the present equipment have been made with other systems.

II.3 External error estimate

The most appropriate way to estimate the external error for a transmissometer system is to determine, either empirically by informed guesses or by calculation, the errors associated with each step of the measurement procedure. Those errors can be combined according to the sum of the squares method. If the individual errors are independent and symmetrical then the resultant error is given by:

$$e_T^2 = \sum_{j=1}^{N} \left(\frac{\partial T_{eff}}{\partial x_j} \right)^2 e_j^2 \qquad \text{(II.1)}$$

where T_{eff} is a function of individual terms in the basic measurement equation each of which contributes some error to the resultant x_j represents the j^{th} parameter in T_{eff} and e_j is the j^{th} error component ($= \frac{\Delta x_j}{x_j}$). Thus the total relative error (%) in T_{eff} is given by

$$E_T^2 = \frac{1}{T_{eff}^2} \sum_{j=1}^{N} \left(\frac{\Delta T_{eff}}{\Delta x_j} \right)^2 e_j^2 * 100 \qquad (II.2)$$

where $T_{eff} = f(x_1, x_2 \ldots x_N)$

E_T as computed above gives the lower bound of the expected error, ie the relative error is not likely to be less than the value given by equation (II.2). The maximum error of the resultant error will occur when all of the error components add up in the same direction and will give an upper bound to the overall error estimate, ie

$$E_{T_{MAX}} = \frac{1}{T_{eff}} \sum_{j=1}^{N} \frac{\Delta T_{eff}}{\Delta x_j} \cdot e_j * 100 \qquad (II.3)$$

It is expected that this upper limit on the total relative error would occur only a small percentage of the time.

The basic *measurement* equation which provides the actually measured effective transmittance (T_{eff}) from instrumentation parameters was derived in Appendix I and is repeated below.

$$T_{eff} = \frac{\epsilon W_{\Delta\lambda} R_M}{F^2 \epsilon' W'_{\Delta\lambda} A_S} \cdot \frac{R^2 V}{R_{\Delta\lambda} G} \qquad (II.4)$$

Equation (II.4) applies after correct alignment procedures have been made and the radiometer signal has been peaked for a particular spectral filter. The main sources of error entering into the process of making transmittance measurements can be summarised as follows:

(i) Alignment errors during transmission measurements.

(ii) Read out error induced by atmospheric scintillation.

(iii) Gain factor error.

(iv) Calibration errors which include those from black-body source temperature, emissivity, transmittance over short 13 m path, collimating mirror alignment and other geometric errors.

(v) Calibraton errors in the field black-body source which include errors from determination of surface temperature, emissivity and spectral filter curves.

(vi) Radiometer repeatability error which includes errors arising from electronic and detector drift and non-linearity.

To arrive at the resultant error equation E_T using the expression for T_{eff} in equation (II.4), the partial derivatives of T_{eff} must first be calculated and combined with the corresponding individual component errors. If $d\varepsilon/\varepsilon$ is the relative error in the value of the emissivity of the calibration source, etc., then the resultant error equation (II.2) becomes:

$$E_T^2 = \left(\frac{\Delta\varepsilon}{\varepsilon}\right)^2 + \left(\frac{\Delta\varepsilon^1}{\varepsilon^1}\right)^2 + \left(\frac{\Delta R_M}{R_M}\right)^2 + \left(\frac{\Delta G_T}{G_T}\right)^2 + 4\left[\left(\frac{\Delta F}{F}\right)^2 + \left(\frac{\Delta D_S}{D_S}\right)^2 + \left(\frac{\Delta R}{R}\right)^2\right] + \left(\frac{\Delta V}{V}\right)^2 + \left(\frac{\Delta R_{\Delta\lambda}}{R_{\Delta\lambda}}\right)^2 + \left(\frac{\Delta W_{\Delta\lambda}}{W_{\Delta\lambda}}\right)^2 + \left(\frac{\Delta W^1_{\Delta\lambda}}{W^1_{\Delta\lambda}}\right)^2 \quad (II.5)$$

Thus the above equation contains 11 relative error terms which are identified as follows:

$\Delta\varepsilon/\varepsilon$ = relative error in the equation emissivity of the calibration source.

$\Delta\varepsilon^1/\varepsilon^1$ = relative error in the emissivity of the field source.

$\Delta R_m/R_m$ = relative error of the reflectance of the collimating mirror used during calibration.

$\Delta G/G$ = relative error in the gain of the radiometer electronics.

$\Delta D_s/D_s$ = relative error in the field source aperture diameter.

$\Delta F/F$ = relative error in collimator mirror focal length.

$\Delta R/R$ = relative error in the distance between receiver and source.

$\Delta V/V$ = relative error in the measured value of radiometer voltage output for a specific filter/detector combination during transmission measurements arising from atmospheric scintillation and instrument repeatability.

$\Delta R_{\Delta\lambda}/R_{\Delta\lambda}$ = total relative error in determining radiometer responsivity for a particular filter/detector combination during calibration.

$\Delta W_{\Delta\lambda}/W_{\Delta\lambda}$ = total relative error in the determination of spectral radiance from the calibration black-body source.

$\Delta W^1_{\Delta\lambda}/W^1_{\Delta\lambda}$ = total relative error in the determination of spectral radiance from the field black-body source.

The estimation of the relative errors $\Delta W_{\Delta\lambda}/W_{\Delta\lambda}$ and $\Delta W'_{\Delta\lambda}/W'_{\Delta\lambda}$ in the radiant flux from the calibration and field black-body sources respectively, was derived using the square root of the sum of the square of known individual errors which contribute to the resultant error identified with the evaluation of the two integrals, namely:

(i) $\int_{\Delta\lambda} W(\lambda,T)T(\lambda,13)T_F(\lambda)d\lambda$, and

(ii) $\int_{\Delta\lambda} W'(\lambda,T)T_F(\lambda)d\lambda$

Tables II.1(a) and II.1(b) list the nature of the errors, their individual values and the estimated resultant relative error in calibration and field source radiant fluxes, respectively. These two relative errors show a strong wavelength dependence which results when the black-body radiant flux becomes more strongly dependent on a given temperature change towards shorter wavelengths.

The overall magnitude of each of the errors which are independent of transmittance and wavelength are listed in Table II.2(a) while the magnitude of those which are dependent on a particular filter/detector combination are listed in II.2(b). After each of these values is substituted into equation (II.5) the total relative error is calculated and given in the form of square root of the sum of the squares in Table II.3. In a similar manner the maximum error for the system can be calculated using equation (II.3). The resultant error values are also listed in Table II.3.

As most transmittance measurements fell between 0.1 and 0.7 the absolute errors for this range of T_{eff} have been calculated for the three broad spectral regions using the lower bound relative error and are listed in Table II.3.

II.4 Errors in effective extinction coefficient

The transmittance of the atmosphere over a particular wavelength interval $\Delta\lambda$ and pathlength R can be expressed in terms of an effective value of the total extinction coefficient (σ_{eff}) by the following expression:

$$\sigma_{eff} = \frac{\ln(T_{eff})}{R} \qquad (II.6)$$

where R is the pathlength in km.

The total extinction coefficient is in fact the sum of the aerosol extinction coefficient (which only varies slowly with wavelength) and the effective molecular extinction coefficient over $\Delta\lambda$ for the given pathlength.

Now errors in the measurement of transmittance T_{eff} will produce errors in σ_{eff}. Differentiating equation (II.6) with respect to T_{eft} and dividing by T_{eff} gives

$$\frac{d\sigma_{eff}}{\sigma_{eff}} = \frac{1}{\ln(T_{eff})} \frac{d\,T_{eff}}{T_{eff}} \qquad (II.7)$$

where dT_{eff} = error independent of the transmittance (constant error), and

$$\frac{d\,T_{eff}}{T_{eff}} = \text{relative error in the transmittance}$$

When both types of errors are present during transmission measurements, the total error in σ_{eff} for the worst case will be:

$$\frac{d\sigma_{eff}}{\sigma_{eff}} = \frac{1}{\ln(T_{eff})} \left(\frac{d\,T_{eff}}{T_{eff}}\right) + \frac{1}{T_{eff}\ln(T_{eff})} (d\,T_{eff}) \qquad (II.8)$$

The relative transmittance error results from calibration errors, variations in the source during measurements, etc. Errors for which dT_{eff} = constant result from uncertainties in calibration source aperture, gain factor, detector and electronic drift, etc and are independent of T_{eff}. Taking values of $dT_{eff} = 0.04$ and $dT_{eff}/T_{eff} = 0.085$ estimated from Table II.2 as representative of the lower bounds of the constant and relative transmittance errors for the present system, the relationship between errors in effective extinction coefficient and errors in transmittance for the full range of transmittance values is shown in figure II.1. It is immediately evident that small errors in transmittance can lead to large errors in effective extinction coefficients for both high and low values of transmittance. As most of the transmittance values fall between 0.5 and 0.7, the majority of the calculated effective extinction coefficient data would have proportional errors at least between 20% and 40%. Therefore care should be taken in interpreting any conclusions from the measured extinction coefficient data. The error analysis in this section does imply that in making transmittance measurements, pathlength should be selected where transmittance values fall below 60% if the error in σ_{eff} is to be kept to a minimum. This is particularly true for the 3.5 to 4.0 μm region where molecular extinction is generally small.

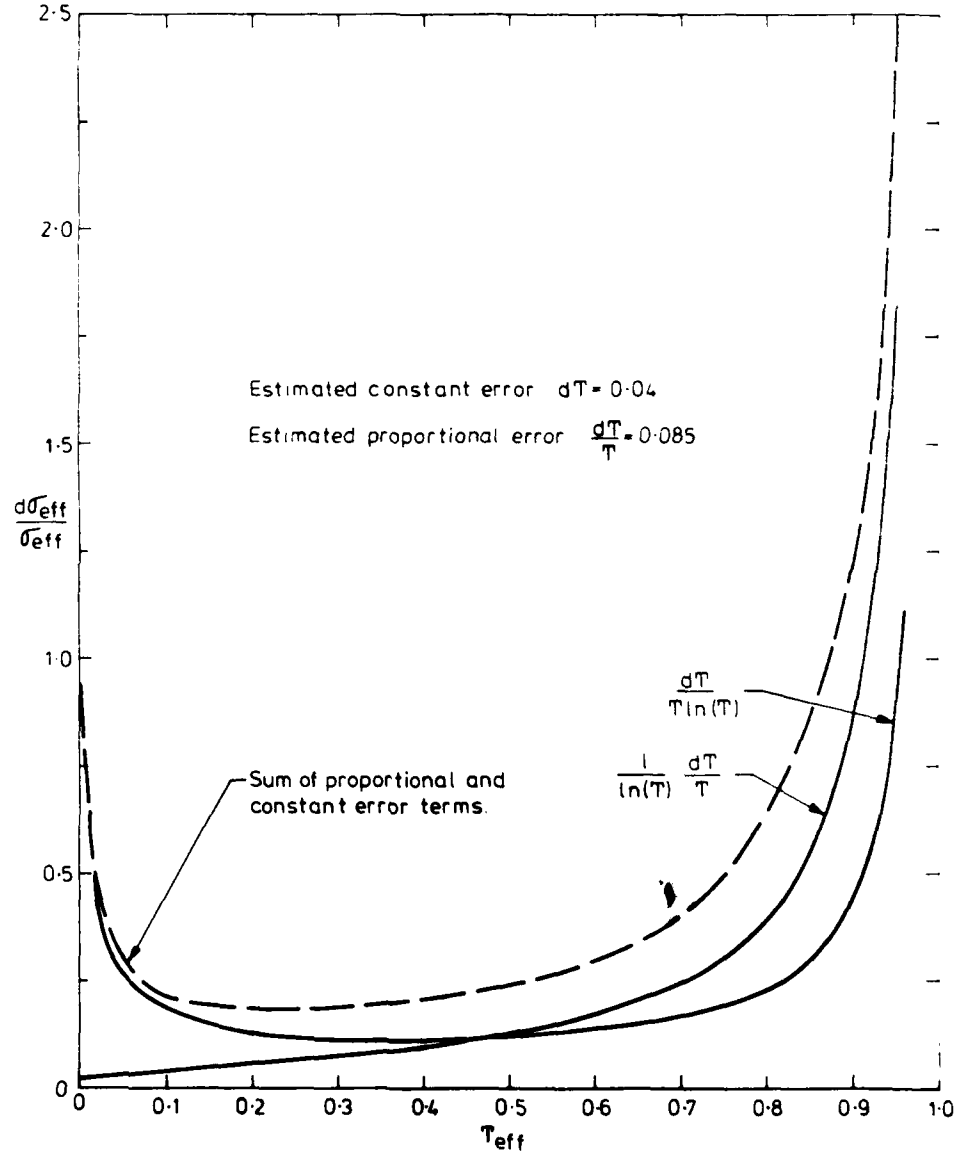

Figure II.1 Proportional error in calculated effective extinction coefficient with measured effective transmittance

TABLE II.1 SUMMARY OF ESTIMATED RELATIVE ERRORS FOR CALIBRATED AND FIELD SOURCES

(a) Calibration Source

Type of Error	Magnitude		
	1 to 3 μm	3 to 5 μm	8 to 12 μm
Numerical integration error in evaluating integral. (A)	0.01	0.01	0.01
Wavelength uncertainty. (B)	0.01	0.01	Negligible
Error in radiant flux due to uncertainty in ave temperature of 2 K. (C)	0.016	0.01	0.005
Uncertainty in calculation of $T(\lambda,13)$. (D)	0.02	0.02	0.01
Estimated resultant relative error = $\sqrt{(A^2+B^2+C^2+D^2)}$	0.029	0.026	0.011

(b) Field source

Type of Error	Magnitude		
	1 to 3 μm	3 to 5 μm	8 to 12 μm
Numerical integration error in evaluating integral. (A)	0.01	0.01	0.01
Wavelength uncertainty. (B)	0.01	0.01	-
Contribution to radiant flux from aperture surround being 10°C above ambient. (C)	-	-	0.005
Error in radiant flux due to uncertainty in ave temperature of 6 K between calibrations. (D)	0.048	0.026	0.013
Estimated resultant relative error = $\sqrt{(A^2+B^2+C^2+D^2)}$	0.050	0.028	0.017

TABLE II.2 SUMMARY OF ESTIMATED INDIVIDUAL ERROR COMPONENTS

(a) Independent of transmittance and wavelength

Relative Error Component	Value	Relative Error Component	Value
$\Delta\varepsilon/\varepsilon$	0.01		
$\Delta\varepsilon^1/\varepsilon^1$	0.02	$\Delta D_s/D_s$	0.018
$\Delta R/R$	0.002	$\Delta F/F$	0.002

(b) Dependent on wavelength and transmittance

Relative Error Component	Magnitude		
	1 to 3 μm	3 to 5 μm	8 to 12 μm
$\Delta V/V$	0.03	0.03	0.03
$\Delta R_{\Delta\lambda}/R_{\Delta\lambda}$	0.02	0.02	0.02
$\Delta R_m/R_m$	0.05	0.07	0.07
$\Delta G/G$	0.01	0.006	0.013
$\Delta W_{\Delta\lambda}/W_{\Delta\lambda}$*	0.029	0.026	0.011
$\Delta W^1_{\Delta\lambda}/W^1_{\Delta\lambda}$*	0.050	0.028	0.017

*Refer to Table II.1

TABLE II.3 SUMMARY OF ESTIMATED RESULTANT TRANSMITTANCE ERRORS

Type of Error	Magnitude		
	1 to 3 μm	3 to 5 μm	8 to 12 μm
Lower bound relative error (Square root of sum of squares)	0.095	0.097	0.093
Upper bound relative error	0.241	0.232	0.213
Absolute error (for $0.1 <= T_{eff} <= 0.7$ with lower bound relative error)		0.01 to 0.07	

DISTRIBUTION

	Copy No.
EXTERNAL	
In United Kingdom	
Defence Science Representative, London	No copy
British Library, Lending Division, Boston Spa, Yorkshire	1
Dr W.A. Shand, RSRE, Pershore	2
In United States of America	
Counsellor, Defence Science, Washington	No copy
Dr G. Trusty, Optical Sciences Division, Naval Research Laboratory, Washington DC	3
Dr R. Fenn, Optical Physics Division, Air Force Geophysics Laboratory, Hanscom, Massachusetts	4
Mr G. Matthews, Electromagnetics Division, Pacific Missile Test Centre, Point Mugu, California	5
Dr H. Hughes, Electromagnetic Propagation Division, Naval Ocean Systems Center, San Diego, California	6
NASA Scientific and Technical Information Office	7
Cambridge Scientific Abstracts	8
In Canada	
Dr W. Tam, Electro-Optics Division, Defence Research Establishment, Valcartier, Quebec	9
In Australia	
Chief Defence Scientist	
Deputy Chief Defence Scientist	10
Superintendent, Science and Technology Programmes	
Controller, Projects and Analytical Studies	
Director, Industry Development, Regional Office, Adelaide	No copy
Director, International Programmes	11
Navy Scientific Adviser	12
Army Scientific Adviser	13
Air Force Scientific Adviser	14

Director, Joint Intelligence Organisation (DSTI) 15

Defence Library, Campbell Park 16

Library, Aeronautical Research Laboratories 17

Library, Materials Research Laboratories 18

Document Exchange Centre
Defence Information Services Branch (for microfilming) 19

Document Exchange Centre
Defence Information Services Branch for:

United Kingdom, Defence Research Information Centre 20

United States, Defense Technical Information Center 21 - 32

Canada, Director Scientific Information Services 33

New Zealand, Ministry of Defence 34

Australian National Library 35

Library, H block, Victoria Barracks, Melbourne 36

Director General, Army Development (NSO), Russell Offices
for ABCA Standardisation Officers

UK ABCA representative, Canberra 37

US ABCA representative, Canberra 38

Canada ABCA representative, Canberra 39

NZ ABCA representative, Canberra 40

WITHIN DRCS

Director, Electronics Research Laboratory 41

Superintendent, Electronic Warfare Division 42

Superintendent, Optoelectronics Division 43

Superintendent, Weapon Systems Division 44

Senior Principal Research Scientist, Surveillance 45

Principal Officer, Electrooptics Group 46

Principal Officer, Infrared and Optical Countermeasures Group 47

Principal Officer, Night Vision Group 48

Principal Officer, Optical Techniques Group 49

Principal Officer, Surveillance Systems Group 50

Principal Officer, Terminal Guidance Group	51
Mr G. McQuistan, Night Vision Group	52
Mr M. Meharry, Night Vision Group	53
Mr I.B. Russo, Optical Techniques Group	54
Author	55 - 56
DRCS Library	57 - 58
Spares	59 - 71

DOCUMENT CONTROL DATA SHEET

Security classification of this page: UNCLASSIFIED

1 DOCUMENT NUMBERS

AR Number: AR-003-098

Series Number: ERL-0265-TR

Other Numbers:

2 SECURITY CLASSIFICATION

a. Complete Document: Unclassified

b. Title in Isolation: Unclassified

c. Summary in Isolation: Unclassified

3 TITLE

ATMOSPHERIC IR TRANSMISSION DATA FOR A TEMPERATE MARITIME ENVIRONMENT

4 PERSONAL AUTHOR(S):

D.R. Cutten

5 DOCUMENT DATE

February 1983

6 6.1 TOTAL NUMBER OF PAGES 61

6.2 NUMBER OF REFERENCES 19

7 7.1 CORPORATE AUTHOR(S):

Electronics Research Laboratory

7.2 DOCUMENT SERIES AND NUMBER

Electronics Research Laboratory 0265-TR

8 REFERENCE NUMBERS

a. Task: DST 78/165

b. Sponsoring Agency:

9 COST CODE

380590

10 IMPRINT (Publishing organisation)

Defence Research Centre Salisbury

11 COMPUTER PROGRAM(S) (Title(s) and language(s))

12 RELEASE LIMITATIONS (of the document):

Approved for Public Release

Security classification of this page: UNCLASSIFIED

Security classification of this page: UNCLASSIFIED

13 ANNOUNCEMENT LIMITATIONS (of the information on these pages)

No limitation

14 DESCRIPTORS:		15 COSATI CODES
a. EJC Thesaurus Terms	Transmittance Interfaces Air water interactions	20140
b. Non-Thesaurus Terms	Infrared transmission Atmospheric transmittance IR atmospheric transmittance	

16 SUMMARY OR ABSTRACT:
(if this is security classified, the announcement of this report will be similarly classified)

Measurements are reported on infrared transmission through the atmosphere at a coastal marine site in a temperate environment. Ten broadband spectral regions were used and variations of transmittance with absolute humidity and visibility over paths of 5 and 9 km investigated. All data have been compared with the predictions of the AFGL computer code LOWTRAN 5. The discrepancy reported previously between the measured and calculated data in the 4.4 to 5.4 μm region still exists, although new data on the water continuum absorption coefficients for this region have reduced this. Reasonable agreement has been shown to exist in the 8 to 12 μm region for absolute humidities up to 12 gm/m^3. The results of the comparisons for the 1 to 2.5 μm region showed a greater discrepancy. Some of this discrepancy could be arising from point measurements of aerosol extinction using equipment which is underestimating the aerosol attenuation coefficient. Data on scintillation fluctuations recorded during the transmittance measurements are also presented.

Security classification of this page: UNCLASSIFIED

The official documents produced by the Laboratories of the Defence Research Centre Salisbury are issued in one of five categories: Reports, Technical Reports, Technical Memoranda, Manuals and Specifications. The purpose of the latter two categories is self-evident, with the other three categories being used for the following purposes:

Reports	:	documents prepared for managerial purposes.
Technical Reports	:	records of scientific and technical work of a permanent value intended for other scientists and technologists working in the field.
Technical Memoranda	:	intended primarily for disseminating information within the DSTO. They are usually tentative in nature and reflect the personal views of the author.

END

DATE
FILMED

9 - 83

DTIC